Research Article

Nonlinear Dynamics of Cutting Process considering Higher-Order Deformation of Composite Cutting Tool

Donghui Yao [ID], Yongsheng Ren [ID], Yuhuan Zhang [ID], and Bole Ma [ID]

College of Mechanical and Electronic Engineering, Shandong University of Science and Technology, Qingdao 266590, China

Correspondence should be addressed to Yongsheng Ren; renys@sdust.edu.cn

In this paper, the nonlinear dynamic analysis of the cutting process of composite cutting tool is performed. The cutting tool is simplified to a nonplanar bending rotating shaft. The higher-order bending deformation, structural damping, and gyroscopic effect of cutting tool are considered. It is assumed that cutting tool is subjected to a regenerative two-dimensional cutting force containing the first and second harmonic components. Based on the Hamilton principle, the motion equation of nonlinear chatter of the cutting system is derived. The nonlinear ordinary differential equations in the generalized coordinates are obtained by Galerkin method. In order to analyze the nonlinear dynamic response of cutting process, the multiscale method is used to derive the analytical approximate solution of the forced response for the cutting system under periodic cutting forces. In the forced response analysis, four cases including primary resonance and superharmonic resonance, i.e., $\overline{\Omega} = \omega_1$, $\overline{\Omega} = \omega_2$, $2\overline{\Omega} = \omega_1$, and $2\overline{\Omega} = \omega_2$, are considered. The influences of ratio of length to diameter, structural damping, cutting force, and ply angle on primary resonance and superharmonic resonance are investigated. The results show that nonlinearity due to higher-order bending deformation significantly affects the dynamic behavior of the milling process and that the effective nonlinearity of the cutting system is of hard type. Multivalued resonance curves and jump phenomenon are presented. The influences of various factors, such as ratio of length to diameter, ply angle, structural damping, cutting force, and rotating speed, are thoroughly discussed.

1. Introduction

As a high-efficiency, high-quality, low-cost machining method, high-speed cutting technology has been widely used in aerospace and mold manufacturing. However, chatter reduces the cutting stability during machining operations, causes a decrease in the machining quality and cutting efficiency of the workpiece, damages the tool, and shortens the service life of the machine.

The passive chatter control methods are mainly based on various types of dynamic vibration absorbers [1, 2] and impact dampers [3]. However, composite materials are known to have higher static stiffness, damping, and specific stiffness. It has been found that the dynamic stiffness and fundamental natural frequency of cutter bar may be improved simultaneously if composite is employed [4–6]. This is very beneficial for the stability of high rotational speed machining for deep holes.

Within the framework of linear chatter theories and based on different theories, several of chatter phenomena as well as their stability boundary in different cutting processes were discovered [7–14]. Tobias [8] introduced the time-delay instability in the cutting force and proposed the regeneration theory, which is considered to provide a complete explanation of the chatter phenomenon so far.

However, because linear theory cannot predict some important dynamic behaviors of cutting process, nonlinear modeling of cutting systems has received more attention. The nonlinearity in cutting systems is mainly caused by structural nonlinearity, delayed nonlinearity of cutting force, etc. [15–18]. Hanna and Tobias [15] first proposed a time-delay nonlinear model with quadratic and cubic structural stiffness and cutting forces, which has inspired great interest in analyzing the global dynamics of the cutting system. The effective mathematical methods for the nonlinear theory of cutting systems include center manifold theory, bifurcation

theory, perturbation analysis, phase portraits, and Poincaré sections.

Pratt [19] used the multiscale method, harmonic balance method, and Floquet theory to study the models of Hanna and Tobias [18]. The results showed that subcritical Hopf bifurcation may occur due to the existence of cubic structural nonlinearity. Moradi et al. [20] studied the existence of different types of bifurcation in the cutting process considering the tool wear and process damping. They developed a 2-dof linear model of the tool and a polynomial nonlinear model of the cutting force. In addition, the multiscale method was used to obtain the approximation analysis solution of primary resonance. Moradi et al. [21] used a model similar to that in literature [20] to analyze the forced vibration of the milling process. In the study, not only the primary resonance but also the superharmonic resonance and the internal resonance were investigated. Moradi et al. [22] investigated the internal resonance and regenerative chatter of the milling process considering both the cutting force and the structural nonlinearity.

However, in the above studies, the tool structure was simulated with 1-dof or 2-dof vibration system, in which the concentration parameters such as mass and stiffness were obtained through experiments or empirical method. There is no obvious correlation between these simplified models and the continuous system equations of the tool.

In order to investigate the dynamic characteristics of cutting system and the stability mechanism of machining process, it is necessary to conduct a comprehensive analysis on various influencing factors. In this case, if the empirical method is used to establish the model of the tool structure, a large number of repetitive tests are needed to obtain the dynamic parameters of the tool structure of different sizes, geometries, and materials, which is very time consuming and of low effectiveness. Therefore, as a more effective modeling method for cutting tool, the continuous parameter dynamics modeling of cutting tool based on analytical method, has received great attention [23–33].

However, in most of the existing continuous system dynamics models, the influence of the nonlinearity of the tool structure has not been considered. Therefore, the existing dynamic model is only suitable for analyzing the linear dynamics of the natural frequency, chatter frequency, dynamic deformation, and chatter stability of the cutting system. In addition, the current continuous system dynamic studies are mainly focused on the tool structure made of isotropic metal materials. Nevertheless, there is no research about the nonlinear dynamics of the process with anisotropy composite tool structures.

The structural nonlinearity is essentially arisen by the flexible nature of the cutting tools with small diameter or long extension part. The structural nonlinearity of the cutting tools may be described using higher-order large deformations [34] or geometric nonlinearity [35].

In this paper, the nonlinear dynamics of the cutting process with a composite cutting tool are investigated. The composite tool structure is simplified to a nonplanar cantilever rotating shaft. The structural nonlinearity is introduced by considering the higher-order deformation of cutting tool. It is assumed that the cutting tool is subjected to a regenerative cutting force containing harmonic components. Based on the Hamilton principle, the nonlinear chatter equation of the cutting system is derived. The Galerkin method is used to obtain the nonlinear ordinary differential equations in the generalized coordinates. The multiscale method is used to obtain the approximate solution of the forced vibration response of the cutting process subjected to periodic cutting forces. Nonlinear dynamics of the system are studied for four cases of primary and superharmonic resonances; i.e., $\overline{\Omega} = \omega_1$, $\overline{\Omega} = \omega_2$, $2\overline{\Omega} = \omega_1$, and $2\overline{\Omega} = \omega_2$ are studied. The numerical calculation is conducted to investigate the effect of various parameters on the frequency response of the cutting system.

2. Mathematical Model and Solution

2.1. Kinetic Energy and Potential Energy. The structural sketch of composite cutting tool with nonplanar bending is shown in Figure 1. The kinetic energy of the rotating cutting tool without considering torsional deformation is as follows:

$$T = \frac{1}{2} \int_0^l \left[\rho A (\dot{v}^2 + \dot{w}^2) + \rho I (\dot{\psi}_y^2 + \dot{\psi}_z^2) - 4\Omega\rho I \psi_z \dot{\psi}_y \right] dx,$$

(1)

where v and w represent the displacement at any point on the neutral axis along the y and z directions, respectively. ψ_z and ψ_y represent bending rotation angles of the cross section around the y and z axes, respectively. ρA represents the mass per unit length, and ρI represents the mass moment of inertia of the cross section. The superposed dots represent derivatives with respect to the time t.

Using the expression of the displacement fields for Euler–Bernoulli beam and the stress-strain displacement relations of the composite cutting tool, as shown in Appendix A, one can obtain the following expression for the potential energy of the rotating composite cutting tool with the higher-order deformation:

$$U = \frac{1}{2} \int_0^L \iint_A \overline{Q}_{11} \left(z^2 \left(\frac{\partial \psi_y}{\partial x} \right)^2 + y^2 \left(\frac{\partial \psi_z}{\partial x} \right)^2 - 2yz \frac{\partial \psi_y}{\partial x} \frac{\partial \psi_z}{\partial x} + \frac{1}{4}\psi_y^4 + \frac{1}{4}\psi_z^4 + \frac{1}{2}\psi_y^2\psi_z^2 - 2\left(z \frac{\partial \psi_y}{\partial x} + y \frac{\partial \psi_z}{\partial x} \right) \left(\frac{1}{2}\psi_y^2 + \frac{1}{2}\psi_z^2 \right) \right)^2 dA dx,$$
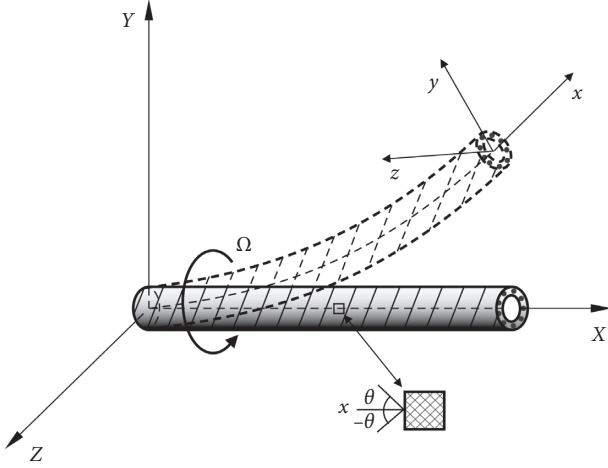
(2)

FIGURE 1: Composite cutting tool with nonplanar bending.

where $\overline{Q}_{11}$ refers to the off-axis stiffness coefficient of the kth layer for the composite cutting tool.

Regardless of the influence of shear deformation, based on the Euler–Bernoulli beam theory, the bending rotation angles and the displacements have the following relationship:

$$\psi_z = -\frac{\partial w}{\partial x}, \psi_y = \frac{\partial v}{\partial x}. \tag{3}$$

2.2. Damping Dissipative Energy Function and Virtual Work of Cutting Force.
Rayleigh dissipative energy function of the cutting tool can be expressed as follows:

$$W_c = \frac{1}{2} \int_0^L c(\dot{v}^2 + \dot{w}^2)dx, \tag{4}$$

where c is structural damping coefficient.

The virtual work of the cutting force δW can be expressed as

$$\delta W = \int_0^L (L_v \delta v + L_w \delta w)dx, \tag{5}$$

where $L_v = F_y \delta_D(x - L)$, $L_w = F_z \delta_D(x - L)$, and $\delta_D(x - L)$ is the delta function.

The linear regenerative cutting forces F_y and F_z can be obtained by [20]

$$F_y = -\frac{N}{2\pi}\left[\alpha_0(v - v_\tau) + \beta_0(w - w_\tau) + \gamma_0\right] + \frac{c_f}{2}\left[\varsigma_1 \cos(2\Omega t - \pi/2) - \eta_1 \cos 2\Omega t + \eta_1\right] + \left[\eta_2 \cos(\Omega t - \pi/2) + \varsigma_2 \cos \Omega t\right],$$

$$F_z = \frac{N}{2\pi}\left[\alpha_0'(v - v_\tau) + \beta_0'(w - w_\tau) + \gamma_0'\right] + \frac{c_f}{2}\left[\eta_1 \cos(2\Omega t - \pi/2) + \varsigma_1 \cos 2\Omega t - \varsigma_1\right] + \left[\varsigma_2 \cos(\Omega t - \pi/2) - \eta_2 \cos \Omega t\right], \tag{6}$$

where

$$\alpha_0 = 0.5\varsigma_1 + 0.25\pi\eta_1, \beta_0 = 0.5\eta_1 + 0.25\pi\varsigma_1,$$
$$\alpha_0' = -0.5\eta_1 + 0.25\pi\varsigma_1, \beta_0' = 0.5\varsigma_1 - 0.25\pi\eta_1,$$
$$\gamma_0 = \eta_2 + \varsigma_2, \gamma_0' = \varsigma_2 - \eta_2,$$
$$\varsigma_1 = K_{tc}a, \varsigma_2 = K_{te}a,$$
$$\eta_1 = K_{rc}a, \eta_2 = K_{re}a,$$
$$v = v(x,t), v_\tau = v(x,t-\tau), w = w(x,t), w_\tau = w(x,t-\tau), \tag{7}$$

in which $\tau = 2\pi/N\Omega$ is the delay time of milling process; N is the number of teeth; (K_{tc}, K_{te}) and (K_{rc}, K_{re}) are the cutting force coefficients in the tangential and radial directions, respectively; a is the axial cutting depth; and c_f is the feed per tooth per revolution.

2.3. Dynamic Model of Milling Process.
In order to obtain the equation of motion of the cutting system, the principle of Hamilton is used as follows:

$$\int_{t_1}^{t_2} (\delta U + \delta W_c - \delta T - \delta W)dt = 0. \tag{8}$$

Substituting (1), (2), (4), and (5) into (8), the equations of motion in both y and z directions can be obtained:

$$(m)_{equiv}\ddot{v} + c\dot{v} - 2(\rho I)_{equiv}\Omega\ddot{w}'' - (\rho I)_{equiv}\ddot{v}'' + (EI)_{equiv}\frac{\partial^4 v}{\partial x^4} + \frac{(EA)_{equiv}}{2}\left[\left(v'^2 + w'^2\right)v'\right]' = F_y\delta_D(x - L),$$

$$(m)_{equiv}\ddot{w} + c\dot{w} + 2(\rho I)_{equiv}\Omega\ddot{v}'' - (\rho I)_{equiv}\ddot{w}'' + (EI)_{equiv}\frac{\partial^4 w}{\partial x^4} + \frac{(EA)_{equiv}}{2}\left[\left(v'^2 + w'^2\right)w'\right]' = F_z\delta_D(x - L), \tag{9}$$

where

$$(m)_{\text{equiv}} = (\rho A)_{\text{equiv}} = \pi \sum_{k=1}^{N} \rho_k \left(r_{k+1}^2 - r_k^2 \right),$$

$$(\rho I)_{\text{equiv}} = \frac{\pi}{4} \sum_{k=1}^{N} \rho_k \left(r_{k+1}^4 - r_k^4 \right),$$

$$(EI)_{\text{equiv}} = \frac{\pi}{4} \sum_{k=1}^{N} \overline{Q}_{11} \left(r_{k+1}^4 - r_k^4 \right), \tag{10}$$

$$(EA)_{\text{equiv}} = \pi \sum_{k=1}^{N} \overline{Q}_{11} \left(r_{k+1}^2 - r_k^2 \right).$$

Here, $(EI)_{\text{equiv}}$ and $(EA)_{\text{equiv}}$ represent the equivalent bending and tensile stiffness of the cutting tool, respectively; $(\rho I)_{\text{equiv}}$ and $(m)_{\text{equiv}}$ represent the equivalent diametrical mass moment of inertia and the equivalent mass per unit length, respectively; ρ_k represents the density of the kth layer; and r_k and r_{k+1} represent the inner diameter and outer diameter of the kth layer, respectively. The detailed expression of $\overline{Q}_{11}$ can be found in Appendix B. In (9), the primes denote differentiation with respect to x.

The following nondimensional quantities are defined:

$$\overline{x} = \frac{x}{L}, \overline{v} = \frac{v}{L}, \overline{w} = \frac{w}{L}, \overline{t} = \sqrt{\frac{(EI)_{\text{equiv}}}{(m)_{\text{equiv}} L^4}} t = \gamma t, \overline{\tau} = \gamma \tau, \overline{c} = \frac{cL^2}{\sqrt{(m)_{\text{equiv}} (EI)_{\text{equiv}}}},$$

$$\overline{\rho I} = \frac{(\rho I)_{\text{equiv}}}{\left((m)_{\text{equiv}} L^2 \right)}, \overline{\Omega} = \sqrt{\frac{(m)_{\text{equiv}} L^4}{(EI)_{\text{equiv}}}} \Omega, \lambda = \frac{(EA)_{\text{equiv}} L^2}{2 (EI)_{\text{equiv}}}, \tag{11}$$

$$\overline{\alpha}_0 = \frac{L^3 \alpha_0}{(EI)_{\text{equiv}}}, \overline{\beta}_0 = \frac{L^3 \beta_0}{(EI)_{\text{equiv}}}, \overline{\gamma}_0 = \frac{L^2 \gamma_0}{(EI)_{\text{equiv}}}, c_{f\varsigma_1} = \frac{L^2 c_f}{(EI)_{\text{equiv}}} \varsigma_1, c_{f\eta_1} = \frac{L^2 c_f}{(EI)_{\text{equiv}}} \eta_1,$$

$$\overline{\alpha}_0' = \frac{L^3 \alpha_0'}{(EI)_{\text{equiv}}}, \overline{\beta}_0' = \frac{L^3 \beta_0'}{(EI)_{\text{equiv}}}, \overline{\gamma}_0' = \frac{L^2 \gamma_0'}{(EI)_{\text{equiv}}}, \overline{\varsigma}_2 = \frac{L^2 \varsigma_2}{(EI)_{\text{equiv}}}, \overline{\eta}_2 = \frac{L^2 \eta_2}{(EI)_{\text{equiv}}}.$$

Using the above dimensionless variables, (9) is rewritten as

$$\ddot{v} + \overline{c} \dot{v} - 2\overline{\rho} \, I \overline{\Omega} \dot{w}'' - \overline{\rho} I \ddot{v}'' + \frac{\partial^4 v}{\partial x^4} + \lambda \left[\left(v'^2 + w'^2 \right) w' \right]' = \overline{F}_y \delta_D (x - 1),$$

$$\ddot{w} + \overline{c} \dot{w} + 2\overline{\rho} I \overline{\Omega} \dot{v}'' - \overline{\rho} I \ddot{w}'' + \frac{\partial^4 w}{\partial x^4} + \lambda \left[\left(v'^2 + w'^2 \right) w' \right]' = \overline{F}_z \delta_D (x - 1), \tag{12}$$

where

$$\overline{F}_y = -\frac{N}{2\pi} \left[\overline{\alpha}_0 (v - v_\tau) + \overline{\beta}_0 (w - w_\tau) + \overline{\gamma}_0 \right] + \frac{1}{2} \left[c_{f\varsigma_1} \cos (2\overline{\Omega}\overline{t} - \pi/2) - c_{f\eta_1} \cos 2\overline{\Omega}\overline{t} + c_{f\eta_1} \right] + \left[\overline{\eta}_2 \cos (2\overline{\Omega}\overline{t} - \pi/2) + \overline{\varsigma}_2 \cos \overline{\Omega}\overline{t} \right],$$

$$\overline{F}_z = \frac{N}{2\pi} \left[\overline{\alpha}_0' (v - v_\tau) + \overline{\beta}' (w - w_\tau) + \gamma_0' \right] - \frac{1}{2} \left[c_{f\eta_1} \cos (2\overline{\Omega}\overline{t} - \pi/2) + c_{f\varsigma_1} \cos 2\overline{\Omega}\overline{t} - c_{f\varsigma_1} \right] + \left[\overline{\varsigma}_2 \cos (2\overline{\Omega}\overline{t} - \pi/2) - \overline{\eta}_2 \cos \overline{\Omega}\overline{t} \right]. \tag{13}$$

In (12), the primes denote differentiation with respect to $\overline{x}$, and the superposed dots denote derivatives with respect to the time $\overline{t}$.

The solution of (12) can be written as

$$v(\overline{x}, \overline{t}) = \phi_1(\overline{x})V(\overline{t}), w(\overline{x}, \overline{t}) = \phi_1(\overline{x})W(\overline{t}). \tag{14}$$

For cantilever beams, $\phi_1(\overline{x})$ has to meet the following boundary conditions:

$$\phi_1(0) = \phi_1'(0) = \phi_1''(1) = \phi_1'''(1) = 0. \tag{15}$$

The mode function that satisfies the boundary condition in (12) can be expressed as follows:

$$\phi_1(\overline{x}) = \cos\beta_1 L\overline{x} - \cosh\beta_1 L\overline{x} - \frac{\cos\beta_1 L + \cosh\beta_1 L}{\sin\beta_1 L + \sinh\beta_1 L}(\sin\beta_1 L\overline{x} - \sinh\beta_1 L\overline{x}), \overline{x} \in (0,1), \tag{16}$$

where $\beta_1 L = 1.875$.

Substituting (14) into (9), simplifying the equation by the Galerkin method, and dropping the constant cutting force terms, the following ordinary differential equations can be obtained.

$$\overline{A}_1\ddot{V} + \overline{A}_2\dot{V} - \overline{A}_3\dot{W} + \overline{A}_4 V + \overline{A}_5 V(V^2 + W^2) = -\frac{N}{2\pi}\left[\overline{\alpha}_0(V - V_\tau) + \overline{\beta}_0(W - W_\tau)\right]\phi_1^2(1) + \overline{F}_{y2}\phi_1(1),$$

$$\overline{A}_1\ddot{W} + \overline{A}_2\dot{W} + \overline{A}_3\dot{V} + \overline{A}_4 W + \overline{A}_5 W(V^2 + W^2) = \frac{N}{2\pi}\left[\overline{\alpha}_0'(V - V_\tau) + \overline{\beta}_0'(W - W_\tau)\right]\phi_1^2(1) + \overline{F}_{z2}\phi_1(1), \tag{17}$$

where

$$\overline{A}_1 = \int_0^1 \phi_1^2(\overline{x})d\overline{x} - \overline{\rho I}\int_0^1 \phi_1(v)\phi_1''(\overline{x})d\overline{x}, \overline{A}_2 = \overline{c}\int_0^1 \phi_1^2(\overline{x})d\overline{x}, \overline{A}_3 = 2\overline{\rho I}\Omega\int_0^1 \phi_1(\overline{x})\phi_1''(\overline{x})d\overline{x},$$

$$\overline{A}_4 = \int_0^1 \phi_1(\overline{x})\phi_1^{(4)}(\overline{x})d\overline{x}, \overline{A}_5 = \lambda\int_0^1 \left(\phi_1'(\overline{x})^3\right)'\phi_1 d\overline{x}. \tag{18}$$

Here, the superscript (4) means the fourth-order partial derivative of $\overline{x}$.

2.4. Perturbation Analysis of Milling Process Using Multiple Scales Method.

In order to solve (17) using the multiscale method, the structural damping and nonlinear and exciting force terms are scaled using small parameters ε as follows:

$$\overline{A}_2 \Rightarrow \varepsilon^2\overline{A}_2, \frac{N}{2\pi}\overline{\alpha}_0 \Rightarrow \varepsilon^2\frac{N}{2\pi}\overline{\alpha}_0, \frac{N}{2\pi}\overline{\beta}_0 \Rightarrow \varepsilon^2\frac{N}{2\pi}\overline{\beta}_0, \frac{N}{2\pi}\overline{\alpha}_0' \Rightarrow \varepsilon^2\frac{N}{2\pi}\overline{\alpha}_0',$$

$$\frac{N}{2\pi}\overline{\beta}_0' \Rightarrow \varepsilon^2\frac{N}{2\pi}\overline{\beta}_0', \overline{F}_{y2} \Rightarrow \varepsilon^3\overline{F}_{y2}, \overline{F}_{z2} \Rightarrow \varepsilon^3\overline{F}_{z2}. \tag{19}$$

$V(\overline{t})$ and $W(\overline{t})$ are expanded in the form

$$V(\overline{t}) = \varepsilon V_1(T_0, T_2) + \varepsilon^3 V_3(T_0, T_2) + \cdots,$$

$$W(\overline{t}) = \varepsilon W_1(T_0, T_2) + \varepsilon^3 W_3(T_0, T_2) + \cdots, \tag{20}$$

where $T_0 = \overline{t}, T_2 = \varepsilon^2\overline{t}$.

Taking the derivative of (20), one obtains the following equations:

$$\dot{V} = \varepsilon\frac{\partial V_1}{\partial T_0} + \varepsilon^3\left(\frac{\partial V_3}{\partial T_0} + \frac{\partial V_1}{\partial T_2}\right) + \cdots,$$

$$\ddot{V} = \varepsilon\frac{\partial^2 V_1}{\partial T_0^2} + \varepsilon^3\left(\frac{\partial^2 V_3}{\partial T_0^2} + 2\frac{\partial^2 V_1}{\partial T_0 \partial T_2}\right) + \cdots,$$

$$\dot{W} = \varepsilon\frac{\partial W_1}{\partial T_0} + \varepsilon^3\left(\frac{\partial W_3}{\partial T_0} + \frac{\partial W_1}{\partial T_2}\right) + \cdots,$$

$$\ddot{W} = \varepsilon\frac{\partial^2 W_1}{\partial T_0^2} + \varepsilon^3\left(\frac{\partial^2 W_3}{\partial T_0^2} + 2\frac{\partial^2 W_1}{\partial T_0 \partial T_2}\right) + \cdots. \tag{21}$$

Substituting (20) and (21) into (17) and considering (19), one can obtain the following equations by comparing the coefficients of ε and ε^3:

O(ε):

$$\overline{A}_1\frac{\partial^2 V_1}{\partial T_0^2} - \overline{A}_3\frac{\partial W_1}{\partial T_0} + \overline{A}_4 V_1 = 0,$$

$$\overline{A}_1\frac{\partial^2 W_1}{\partial T_0^2} + \overline{A}_3\frac{\partial V_1}{\partial T_0} + \overline{A}_4 W_1 = 0. \tag{22}$$

$O(\varepsilon^3)$:

$$\overline{A}_1\frac{\partial^2 V_3}{\partial T_0^2} - \overline{A}_3\frac{\partial W_3}{\partial T_0} + \overline{A}_4 V_3 = -2\overline{A}_1\frac{\partial^2 V_1}{\partial T_0 \partial T_2} - \overline{A}_2\frac{\partial V_1}{\partial T_0} + \overline{A}_3\frac{\partial W_1}{\partial T_2} - \overline{A}_5 V_1\left(V_1^2 + W_1^2\right) - \frac{N}{2\pi}\left[\overline{\alpha}_0\left(V_1 - V_{1\tau}\right) + \overline{\beta}_0\left(W_1 - W_{1\tau}\right)\right]$$

$$\phi_1^2(1) + \lambda_V + \overline{F}_{y2}\phi_1(1),$$

$$\overline{A}_1\frac{\partial^2 W_3}{\partial T_0^2} + \overline{A}_3\frac{\partial V_3}{\partial T_0} + \overline{A}_4 W_3 = -2\overline{A}_1\frac{\partial^2 W_1}{\partial T_0 \partial T_2} - \overline{A}_2\frac{\partial W_1}{\partial T_0} - \overline{A}_3\frac{\partial V_1}{\partial T_2} - \overline{A}_5 W_1\left(V_1^2 + W_1^2\right) + \frac{N}{2\pi}\left[\overline{\alpha}_0'\left(V_1 - V_{1\tau}\right) + \overline{\beta}_0'\left(W_1 - W_{1\tau}\right)\right]$$

$$\phi_1^2(1) + \lambda_W + \overline{F}_{z2}\phi_1(1). \tag{23}$$

Assume the solution of (22) is as follows:

$$V_1(T_0, T_2) = F_1(T_2)e^{i\omega_1 T_0} + F_2(T_2)e^{i\omega_2 T_0} + \overline{F}_1(T_2)e^{-i\omega_1 T_0} + \overline{F}_2(T_2)e^{-i\omega_2 T_0},$$

$$W_1(T_0, T_2) = -iF_1(T_2)e^{i\omega_1 T_0} + iF_2(T_2)e^{i\omega_2 T_0} + i\overline{F}_1(T_2)e^{-i\omega_1 T_0} - i\overline{F}_2(T_2)e^{-i\omega_2 T_0},$$

$$V_{1\tau}(T_0, T_2) = F_1(T_2)e^{i\omega_1(T_0-\overline{\tau})} + F_2(T_2)e^{i\omega_2(T_0-\overline{\tau})} + \overline{F}_1(T_2)e^{-i\omega_1(T_0-\overline{\tau})} + \overline{F}_2(T_2)e^{-i\omega_2(T_0-\overline{\tau})},$$

$$W_{1\tau}(T_0, T_2) = -iF_1(T_2)e^{i\omega_1(T_0-\overline{\tau})} + iF_2(T_2)e^{i\omega_2(T_0-\overline{\tau})} + i\overline{F}_1(T_2)e^{-i\omega_1(T_0-\overline{\tau})} - i\overline{F}_2(T_2)e^{-i\omega_2(T_0-\overline{\tau})}, \tag{24}$$

where $i = \sqrt{-1}$ represents the imaginary unit, $F_1(T_2)$ and $F_2(T_2)$ are the complex functions to be determined, and $\overline{F}_1(T_2)$ and $\overline{F}_2(T_2)$ represent the complex conjugate. ω_1 and ω_2 refer to the forward and backward whirling frequencies, respectively, which are expressed as follows:

$$\omega_1 = \frac{\overline{A}_3 + \sqrt{\overline{A}_3^2 + 4\overline{A}_1\overline{A}_4}}{2\overline{A}_1}, \omega_2 = \frac{-\overline{A}_3 + \sqrt{\overline{A}_3^2 + 4\overline{A}_1\overline{A}_4}}{2\overline{A}_1}. \tag{25}$$

Substituting (24) into (23) and dropping the constant terms λ_V and λ_W, one obtains the following equations:

$$\overline{A}_1\frac{\partial^2 V_3}{\partial T_0^2} - \overline{A}_3\frac{\partial W_3}{\partial T_0} + \overline{A}_4 V_3 = P_3 e^{i\omega_1 T_0} + Q_3 e^{i\omega_2 T_0} + \overline{\overline{F}}_{y2},$$

$$\overline{A}_1\frac{\partial^2 W_3}{\partial T_0^2} + \overline{A}_3\frac{\partial V_3}{\partial T_0} + \overline{A}_4 W_3 = P_4 e^{i\omega_1 T_0} + Q_4 e^{i\omega_2 T_0} + \overline{\overline{F}}_{z2}, \tag{26}$$

where

$$P_3 = \Gamma_1 - i\Lambda_1 F_1' - i\overline{A}_2\omega_1 F_1 - \phi_1^2(1)\frac{N}{2\pi}\left(\overline{\overline{\alpha}}_0 - i\overline{\overline{\beta}}_0\right)\left(1 - e^{-i\omega_1\tau}\right)F_1,$$

$$Q_3 = \Gamma_2 - i\Lambda_2 F_2' - i\overline{A}_2\omega_2 F_2 - \phi_1^2(1)\frac{N}{2\pi}\left(\overline{\overline{\alpha}}_0 + i\overline{\overline{\beta}}_0\right)\left(1 - e^{-i\omega_2\overline{\tau}}\right)F_2,$$

$$P_4 = -i\Gamma_1 - \Lambda_1 F_1' - \overline{A}_2\omega_1 F_1 + \phi_1^2(1)\frac{N}{2\pi}\left(\overline{\overline{\alpha}}_0' - i\overline{\overline{\beta}}_0'\right)\left(1 - e^{-i\omega_1\overline{\tau}}\right)F_1,$$

$$Q_4 = i\Gamma_2 + \Lambda_2 F_2' + \overline{A}_2\omega_2 F_2 + \phi_1^2(1)\frac{N}{2\pi}\left(\overline{\overline{\alpha}}_0' + i\overline{\overline{\beta}}_0'\right)\left(1 - e^{-i\omega_2\overline{\tau}}\right)F_2,$$

$$\Lambda_1 = 2\overline{A}_1\omega_1 + \overline{A}_3, \Gamma_1 = -4\overline{A}_5\left(F_1^2\overline{F}_1 + 2F_1 F_2\overline{F}_2\right),$$

$$\Lambda_2 = 2\overline{A}_1\omega_2 - \overline{A}_3, \Gamma_2 = -4\overline{A}_5\left(F_2^2\overline{F}_2 + 2F_1 F_2\overline{F}_1\right),$$

$$\overline{\overline{F}}_{y_2} = \overline{F}_{y_2}\phi_1(1),$$

$$\overline{\overline{F}}_{z_2} = \overline{F}_{z_2}\phi_1(1). \tag{27}$$

In this paper, four cases of primary and superharmonic resonances, i.e., case I: $\overline{\Omega} = \omega_1$, case II: $\overline{\Omega} = \omega_2$, case III: $2\overline{\Omega} = \omega_1$, and case IV: $2\overline{\Omega} = \omega_2$, are studied.

2.4.1. Case I: Primary Resonance ($\overline{\Omega} = \omega_1$). Assume

$$\overline{\Omega} = \omega_1 + \varepsilon^2 \sigma, \tag{28}$$

where σ represents the detuning parameter.

Substituting (24) into (26), one can obtain the following equations:

$$\overline{A}_1 \frac{\partial^2 V_3}{\partial T_0^2} - \overline{A}_3 \frac{\partial W_3}{\partial T_0} + \overline{A}_4 V_3 = \overline{P}_3 e^{i\omega_1 T_0} + \overline{Q}_3 e^{i\omega_2 T_0},$$

$$\overline{A}_1 \frac{\partial^2 W_3}{\partial T_0^2} + \overline{A}_3 \frac{\partial V_3}{\partial T_0} + \overline{A}_4 W_3 = \overline{P}_4 e^{i\omega_1 T_0} + \overline{Q}_4 e^{i\omega_2 T_0}, \tag{29}$$

where

$$\begin{aligned}
\overline{P}_3 &= P_3 + \phi_1(1)\overline{q}_1 e^{i\sigma T_2}, \\
\overline{P}_4 &= P_4 - i\phi_1(1)\overline{q}_1 e^{i\sigma T_2}, \\
\overline{Q}_3 &= Q_3, \\
\overline{Q}_4 &= Q_4,
\end{aligned} \tag{30}$$

where $\overline{q}_1 = (\overline{\varsigma}_2 - i\overline{\eta}_2)/2$.

The particular solutions of (29) are

$$\begin{aligned}
V_3(T_0, T_2) &= F_{11}(T_2)e^{i\omega_1 T_0} + F_{12}(T_2)e^{i\omega_2 T_0}, \\
W_3(T_0, T_2) &= F_{21}(T_2)e^{i\omega_1 T_0} + F_{22}(T_2)e^{i\omega_2 T_0}.
\end{aligned} \tag{31}$$

Substituting (31) into (29) and equating the coefficient of $e^{i\omega_1 T_0}$ and $e^{i\omega_2 T_0}$ in both sides of (29), one has

$$\begin{aligned}
\left(\overline{A}_4 - \overline{A}_1 \omega_1^2\right)F_{11} - i\overline{A}_3 \omega_1 F_{21} &= \overline{P}_3, \\
i\overline{A}_3 \omega_1 F_{11} + \left(\overline{A}_4 - \overline{A}_1 \omega_1^2\right)F_{21} &= \overline{P}_4.
\end{aligned} \tag{32}$$

$$\begin{aligned}
\left(\overline{A}_4 - \overline{A}_1 \omega_2^2\right)F_{12} - i\overline{A}_3 \omega_2 F_{22} &= \overline{Q}_3, \\
i\overline{A}_3 \omega_2 F_{12} + \left(\overline{A}_4 - \overline{A}_1 \omega_2^2\right)F_{22} &= \overline{Q}_4.
\end{aligned} \tag{33}$$

Equations (32) and (33) constitute systems of two inhomogeneous algebraic equations for F_{11}, F_{21} and F_{12}, F_{22},

respectively. Their homogeneous parts have a nontrivial solution. Then their solvability conditions can be written as [36]

$$\begin{aligned}
\begin{vmatrix} \overline{P}_3 & -i\overline{A}_3\omega_1 \\ \overline{P}_4 & \overline{A}_4 - \overline{A}_1\omega_1^2 \end{vmatrix} &= 0, \\
\begin{vmatrix} \overline{A}_4 - \overline{A}_1\omega_1^2 & \overline{P}_3 \\ i\overline{A}_3\omega_1 & \overline{P}_4 \end{vmatrix} &= 0.
\end{aligned} \tag{34}$$

$$\begin{aligned}
\begin{vmatrix} \overline{Q}_3 & -i\overline{A}_3\omega_2 \\ \overline{Q}_4 & \overline{A}_4 - \overline{A}_1\omega_2^2 \end{vmatrix} &= 0, \\
\begin{vmatrix} \overline{A}_4 - \overline{A}_1\omega_2^2 & \overline{Q}_3 \\ i\overline{A}_3\omega_2 & \overline{Q}_4 \end{vmatrix} &= 0.
\end{aligned} \tag{35}$$

After simplification, the solvability conditions are reduced to two independent governing equations in the following form:

$$4\overline{A}_5\left(F_1^2\overline{F}_1 + 2F_1 F_2 \overline{F}_2\right) - i\Lambda_1 F_1' - i\overline{A}_2 \omega_1 F_1 + \phi_1^2(1)\frac{N}{4\pi}$$

$$\left[\overline{\beta}_0' - \overline{\alpha}_0 + i\left(\overline{\alpha}_0' + \overline{\beta}_0\right)\right]\left(1 - e^{-i\omega_1\overline{\tau}}\right)F_1 + \phi_1(1)\overline{q}_1 e^{i\sigma T_2} = 0, \tag{36}$$

$$4\overline{A}_5\left(F_2^2\overline{F}_2 + 2F_1 F_2 \overline{F}_1\right) - i\Lambda_2 F_2' - i\overline{A}_2 \omega_2 F_2 - \frac{1}{2}\phi_1^2(1)\frac{N}{2\pi}$$

$$\left[\overline{\alpha}_0 + \overline{\beta}_0' + i\left(\overline{\alpha}_0' - \overline{\beta}_0\right)\right]\left(1 - e^{-i\omega_1\overline{\tau}}\right)F_2 = 0. \tag{37}$$

Assume that the solutions of (36) and (37) are

$$\begin{aligned}
F_1 &= \frac{1}{2}a_1(T_2)e^{i\theta_1(T_2)}, \\
F_2 &= \frac{1}{2}a_2(T_2)e^{i\theta_2(T_2)},
\end{aligned} \tag{38}$$

where $a_j(T_2)$ and $\theta_j(T_2)$ ($j = 1,2$) refer to the amplitudes and phase angles of the response, respectively.

Substituting (38) into (36) and (37), separating the real and the imaginary parts, one can obtain the following equations:

$$\Lambda_1 a_1' = -\overline{A}_2 \omega_1 a_1 + \phi_1^2(1)\frac{N}{4\pi}\left(\left(\overline{\alpha}_0' + \overline{\beta}_0\right)\left(1 - \cos\omega_1\overline{\tau}\right) + \left(\overline{\beta}_0' - \overline{\alpha}_0\right)\sin\omega_1\overline{\tau}\right)a_1 + \phi_1(1)\left(\overline{\varsigma}_2 \sin\psi_1 - \overline{\eta}_2 \cos\psi_1\right),$$

$$\Lambda_1 a_1 \psi_1' = \Lambda_1 \sigma a_1 - \overline{A}_5\left(a_1^3 + 2a_1 a_2^2\right) + \phi_1^2(1)\frac{N}{4\pi}\left(\left(\overline{\beta}_0' - \overline{\alpha}_0\right)\left(1 - \cos\omega_1\overline{\tau}\right) - \left(\overline{\alpha}_0' + \overline{\beta}_0\right)\sin\omega_1\overline{\tau}\right)a_1 + \phi_1(1)\left(\overline{\eta}_2 \sin\psi_1 + \overline{\varsigma}_2 \cos\psi_1\right).$$

$$\tag{39}$$

$$\Lambda_2 a_2' = -\overline{A}_2 \omega_2 a_2 - \phi_1^2(1)\frac{N}{4\pi}\left(\left(\overline{\alpha}_0' + \overline{\beta}_0\right)\left(1 - \cos\omega_2\overline{\tau}\right) + \left(\overline{\alpha}_0 - \overline{\beta}_0'\right)\sin\omega_2\overline{\tau}\right)a_2,$$

$$\Lambda_2 \psi_2' a_2 = -\overline{A}_5\left(a_2^3 + 2a_1^2 a_2\right) - \phi_1^2(1)\frac{N}{4\pi}\left(\left(\overline{\alpha}_0 - \overline{\beta}_0'\right)\left(1 - \cos\omega_2\overline{\tau}\right) - \left(\overline{\alpha}_0' + \overline{\beta}_0\right)\sin\omega_2\overline{\tau}\right)a_2,$$

$$\tag{40}$$

where $\sigma T_2 - \theta_j = \psi_j$ $(j = 1,2)$.

To determine the steady-state forced response, the time derivatives in (39) and (40) are set to zero. It can be immediately concluded from (40) that only solution for a_2 is zero. This shows that under the primary resonance $\Omega \approx \omega_1$,

only the first mode, i.e., the forward mode, can be excited, while the second mode, i.e., the backward mode, does not participate in the primary resonance and remains stationary.

Substituting $a_2 = 0$ into (39) and solving for σ, one obtains

$$
\sigma = -\phi_1^2(1) \frac{N}{4\pi\Lambda_1} \left[\left(\overline{\beta}_0' - \overline{\alpha}_0 \right) \left(1 - \cos \omega_1 \overline{\tau} \right) - \left(\overline{\alpha}_0' + \overline{\beta}_0 \right) \sin \omega_1 \overline{\tau} \right] + \frac{\overline{A}_5}{\Lambda_1} a_1^2
$$

$$
\pm \frac{1}{\Lambda_1} \sqrt{ \frac{\phi_1^2(1)\left(\overline{\varsigma}_2^2 + \overline{\eta}_2^2 \right)}{a_1^2} - \left[\overline{A}_2 \omega_1 - \phi_1^2(1) \frac{N}{4\pi} \left[\left(\overline{\alpha}_0' + \overline{\beta}_0 \right) \left(1 - \cos \omega_1 \overline{\tau} \right) + \left(\overline{\beta}_0' - \overline{\alpha}_0 \right) \sin \omega_1 \overline{\tau} \right] \right]^2 }.
\tag{41}
$$

To study the stability of the steady-state response of case I, the nature of steady-state response can be investigated numerically by linearizing (39) (with $a_2 = 0$) around (a_0, ψ_0).

2.4.2. Case II: Primary Resonance $(\overline{\Omega} = \omega_2)$. According to (26), under such conditions, one introduces detuning parameters as

$$
\overline{\Omega} = \omega_2 + \varepsilon^2 \sigma.
\tag{42}
$$

Using their solvability conditions (which are not shown) and (38) leads to

$$
\Lambda_1 a_1' = -\overline{A}_2 \omega_1 a_1 + \phi_1^2(1) \frac{N}{4\pi} \left(\left(\overline{\alpha}_0' + \overline{\beta}_0 \right) \left(1 - \cos \omega_1 \overline{\tau} \right) + \left(\overline{\beta}_0' - \overline{\alpha}_0 \right) \sin \omega_1 \overline{\tau} \right) a_1,
$$

$$
\Lambda_1 a_1 \psi_1' = \Lambda_1 \sigma a_1 - \overline{A}_5 \left(a_1^3 + 2 a_1 a_2^2 \right) + \phi_1^2(1) \frac{N}{4\pi} \left(\left(\overline{\beta}_0' - \overline{\alpha}_0 \right) \left(1 - \cos \omega_1 \overline{\tau} \right) - \left(\overline{\alpha}_0' + \overline{\beta}_0 \right) \sin \omega_1 \overline{\tau} \right) a_1,
$$

$$
\Lambda_2 a_2' = -\overline{A}_2 \omega_2 a_2 - \phi_1^2(1) \frac{N}{4\pi} \left(\left(\overline{\alpha}_0' + \overline{\beta}_0 \right) \left(1 - \cos \omega_2 \overline{\tau} \right) + \left(\overline{\alpha}_0 - \overline{\beta}_0' \right) \sin \omega_2 \overline{\tau} \right) a_2 - \phi_1(1) \left(\overline{\varsigma}_2 \sin \psi_2 - \overline{\eta}_2 \cos \psi_2 \right),
$$

$$
\Lambda_2 \psi_2' a_2 = -\overline{A}_5 \left(a_2^3 + 2 a_1^2 a_2 \right) - \phi_1^2(1) \frac{N}{4\pi} \left(\left(\overline{\alpha}_0 - \overline{\beta}_0' \right) \left(1 - \cos \omega_2 \overline{\tau} \right) - \left(\overline{\alpha}_0' + \overline{\beta}_0 \right) \sin \omega_2 \overline{\tau} \right) a_2 - \phi_1(1) \left(\overline{\varsigma}_2 \cos \psi_2 + \overline{\eta}_2 \sin \psi_2 \right).
\tag{43}
$$

By using steady-state condition (i.e., set $a_1' = 0$, $\psi_1' = 0$, $a_2' = 0$, and $\psi_2' = 0$), the following steady-state response of case II can be obtained:

$$
\sigma = \phi_1^2(1) \frac{N}{4\pi\Lambda_2} \left[\left(\overline{\alpha}_0 - \overline{\beta}_0' \right) \left(1 - \cos \omega_2 \overline{\tau} \right) - \left(\overline{\alpha}_0' + \overline{\beta}_0 \right) \sin \omega_2 \overline{\tau} \right] + \frac{\overline{A}_5}{\Lambda_2} a_2^2
$$

$$
\pm \frac{1}{\Lambda_2} \sqrt{ \frac{\phi_1^2(1)\left(\overline{\varsigma}_2^2 + \overline{\eta}_2^2 \right)}{a_2^2} - \left[\frac{2}{A} \omega_2 + \phi_1^2(1) \frac{N}{4\pi} \left[\left(\overline{\alpha}_0' + \overline{\beta}_0 \right) \left(1 - \cos \omega_2 \overline{\tau} \right) + \left(\overline{\alpha}_0 - \overline{\beta}_0' \right) \sin \omega_2 \overline{\tau} \right] \right]^2 }.
\tag{44}
$$

From (44), it can be seen that $a_1 = 0$ and $a_2 \neq 0$, indicating that only the forced vibration response of backward mode is excited, while forward mode remains stationary.

2.4.3. Case III: Superharmonic Resonance $(2\overline{\Omega} = \omega_1)$. For this case, the formulation of steady-state response is the same as case I, but in (41), $\overline{\varsigma}_2$ and $\overline{\eta}_2$ are replaced with $c_{f\varsigma_1}/2$ and $c_{f\eta_1}/2$, respectively.

2.4.4. Case IV: Superharmonic Resonance ($2\overline{\Omega} = \omega_2$). For this case, the formulation of steady-state response is the same as case II, but in (43), $\overline{\varsigma}_2$ and $\overline{\eta}_2$ are replaced with $c_{f\varsigma_1}/2$ and $c_{f\eta_1}/2$, respectively.

3. Numerical Results and Discussions

In this study, the composite material of carbon fiber/epoxy resin is selected as the material of the cutting tool. The mechanical properties of the material are shown in Table 1. Coefficients of cutting forces for simulation are given in Table 2. The cutting tool has a hollow structure, the outer diameter of the cross section is $D = 8$ mm, the inner diameter is $D = 4$ mm, the thickness of the section is $h = 2$ mm, and the length L is determined by the given ratio of length to diameter. The composite cutting tool has 16 layers with identical thickness, and the stack sequence is $[\pm\theta]_8$. In all cases, $\overline{\Omega} = 200$, except where other values are mentioned.

Figure 2 shows the natural frequency versus rotating speed, which is generally known as a Campbell diagram. In vibration of gyroscopic systems, there are two natural frequencies associated with forward and backward whirling motions. In forward natural frequency, the natural frequency is measured when the rotating cutting tool whirls in direction of the rotation. However, in backward natural frequency, the natural frequency is measured when the cutting tool whirls in the opposite direction of the rotation. The forward natural frequency (black solid line) increases with the increase of the rotating speed, while the backward natural frequency (blue dashed line) decreases with the increase of the rotating speed. The intersections of the curves related to the natural frequencies with the straight line $\omega_n = \overline{\Omega}$ determine the critical rotating speeds of the rotating cutting tool.

3.1. Stability Lobe Diagram. By removing the nonlinear term and the harmonic cutting force in the right-side term of (17), the stability of the cutting system can be investigated. Figure 3 shows a stability lobe diagram where the Ω versus a_{lim} curve separates the space into two regions. Any (Ω, a_{lim}) pair that appears above the collective boundary indicates unstable milling process where regenerative chatter or self-excited vibration occurs, while any pair below the boundary is a stable milling process.

3.2. Primary Resonance Response

3.2.1. Case I. The numerical solutions for the forced vibration responses of the cutting system with composite cutting tool are presented in Figure 4. As shown in Figure 4, by increasing detuning parameters at point A, the amplitude a_1 gradually increases until reaching point B. a_1 jumps downward from point B to point C. Afterward, a_1 gradually drops to point D while continuing increasing the detuning parameter. On the other hand, as the detuning parameter decreases from point D to point E, a_1 increases and jumps upward from point E to point F. As the detuning parameter further decreases, a_1 drops until arriving at point A. By

TABLE 1: Mechanical properties of carbon fiber/epoxy composite [37].

ρ(kg/m³)	E_{11} (GPa)	E_{22} (GPa)	G_{12} (GPa)	G_{23} (GPa)	ν_{12}
1672	25.8	8.7	3.5	3.5	0.34

TABLE 2: Coefficients of cutting forces [21].

C_f (mm/rev-tooth)	$\overline{\overline{\varsigma}}_1$ (N/mm)	$\overline{\overline{\eta}}_1$ (N)	$\overline{\overline{\varsigma}}_2$ (N/mm)	$\overline{\overline{\eta}}_2$ (N)	a_c (mm)	N
0.2	620	208	43	52	3	4
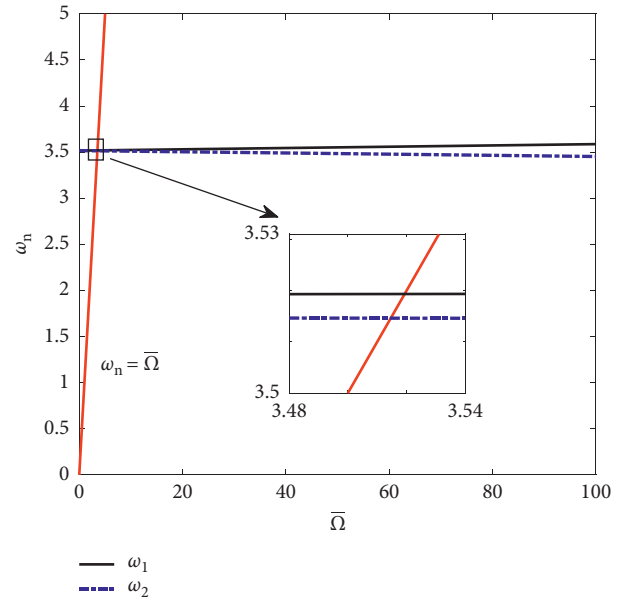
FIGURE 2: Natural frequency versus rotational speed (L/d = 10, $\theta = 0°$).
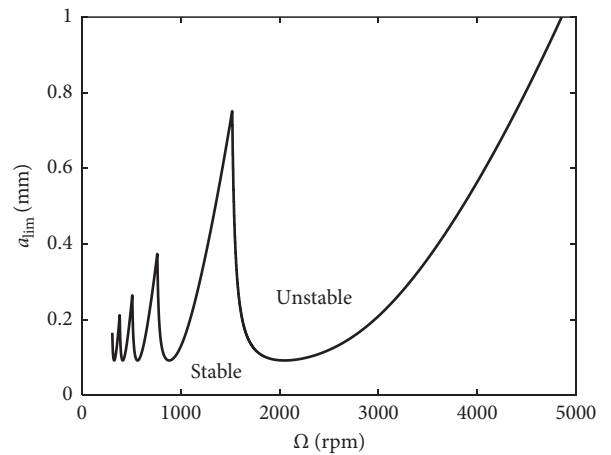
FIGURE 3: Stability lobe diagram of the cutting system with composite cutting tool (L/d = 10, $\overline{c} = 0.3$, $\theta = 0°$).

considering the nonlinearity of higher-order bending deformation, the forced response curve of the cutting system deviates toward the right, suggesting hard spring vibration
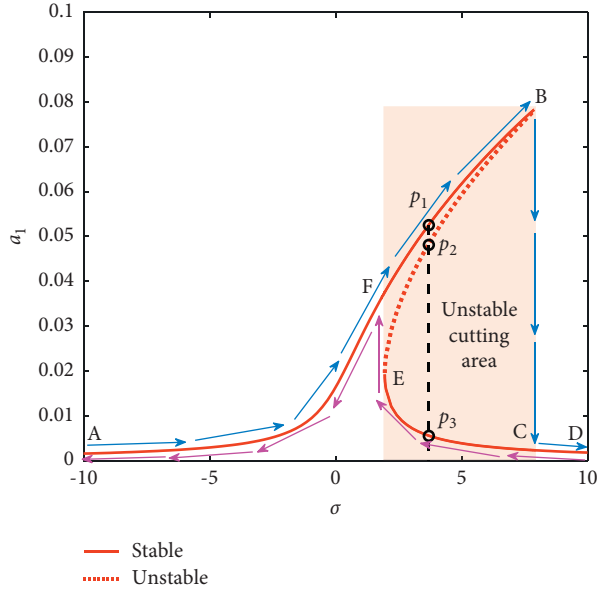
FIGURE 4: Frequency response curve in case I.

FIGURE 5: The effect of ratio of length to diameter on frequency response curve ($\bar{c} = 0.01$, $\theta = 0°$, case I).

FIGURE 6: The effect of structural damping on frequency response curve (L/d = 10, $\theta = 0°$, case I).

behavior of Duffing type oscillator. As the detuning parameter varies between σ_F and σ_B, the cutting system has three steady-state vibration amplitudes, p_1, p_2, and p_3, among which p_1 and p_3 are stable and p_2 is unstable. This means that the cutting system works in an unstable cutting state. Therefore, cutting conditions and consequently initial conditions should be adjusted such that the stable branch with less vibration amplitudes is realized in practice.

Figures 5–9 show the effects of ratio of length to diameter, structural damping, cutting force, ply angle, and rotating speed on frequency response curve, respectively, for the case $\overline{\Omega} = \omega_1$. As shown in Figure 5, when ratio of length to diameter increases, vibration amplitudes decrease and frequency response curve bends more strongly toward left. This is physically expected, because the nonlinear stiffness coefficient $\lambda = (EA)_{equiv} L^2/2 (EI)_{equiv}$ is proportional to ratio of length to diameter according to (12). As is observed and physically expected from Figure 6, the increase in the structural damping leads to the decrease in vibration amplitudes. In order to study the effect of cutting force coefficients, we define $\varsigma_2 = K_f \overline{\overline{\varsigma}}_2$, $\eta_2 = K_f \overline{\overline{\eta}}_2$, with the parameters $\overline{\overline{\varsigma}}_2$ and $\overline{\overline{\eta}}_2$ given in Table 2. As is shown in Figure 7, by increasing cutting forces, vibration amplitudes increase. Figure 8 shows that the primary resonance amplitude increases with the increase of the ply angle because the elastic modulus E_{11} along the longitudinal direction of the fiber is significantly larger than the transverse elastic modulus E_{22} (as shown in Table 1). Therefore, as the ply angle is greater, the equivalent bending stiffness $(EI)_{equiv}$ of the composite cutting tool is smaller; thus, the nondimensional cutting force coefficients are greater (as shown in (11)). As a result, the amplitude of the primary resonance response is larger.

Figure 9 shows that vibration amplitudes decrease with the decrease of rotating speed. This is physically expected, because the equivalent damping of the cutting system (which will be introduced in the subsequent section) increases with
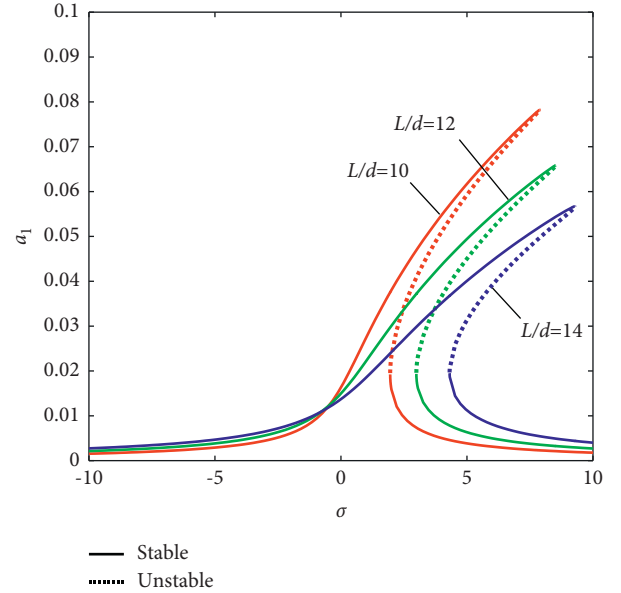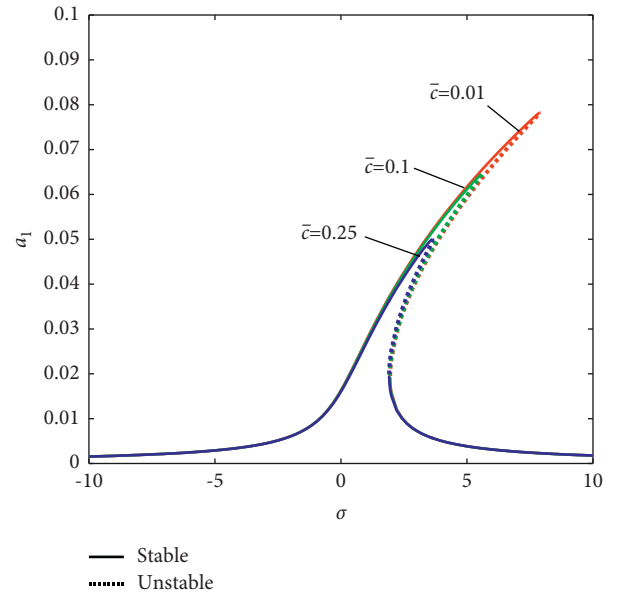
the decrease of rotating speed due to the damping effect from regenerative chatter mechanism.

Figures 10–14 show the amplitude versus damping coefficient with different ratios of length to diameter, detuning parameter values, cutting force coefficients, ply angles, and rotating speeds, respectively, for the case $\overline{\Omega} = \omega_1$. From these figures, it can be seen that for some values of L/d, σ, K_f, or θ, there are multivalued curves. For example, when $L/d = 10$ and $\bar{c} < 0.45$, as is shown in Figure 10, the system has two stable and one unstable branches, but for $L/d = 10$ and $\bar{c} > 0.45$, there exists only
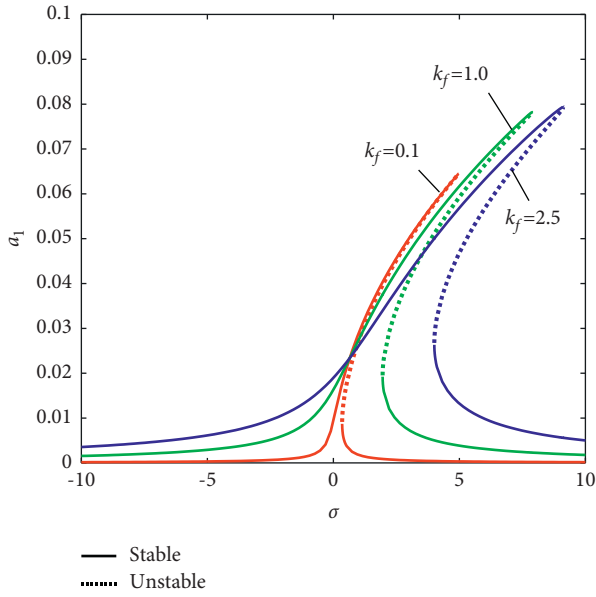
FIGURE 7: The effect of cutting force coefficient on frequency response curve (L/d = 10, $\bar{c}$ = 0.01, θ = 0°, case I).
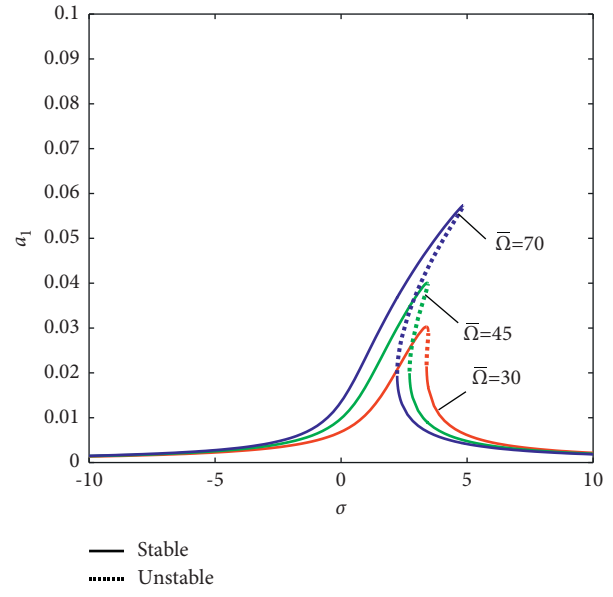
FIGURE 9: The effect of rotating speed on frequency response curve (L/d = 10, $\bar{c}$ = 0.01, θ = 0°, case I).
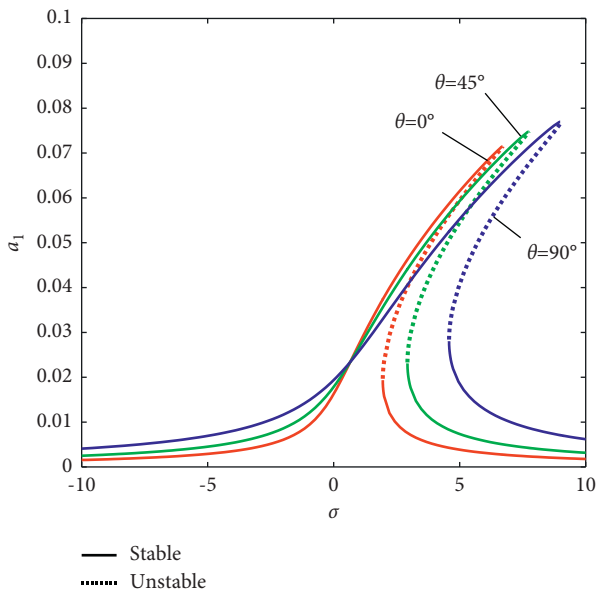
FIGURE 8: The effect of ply angle on frequency response curve (L/d = 10, $\bar{c}$ = 0.01, case I).
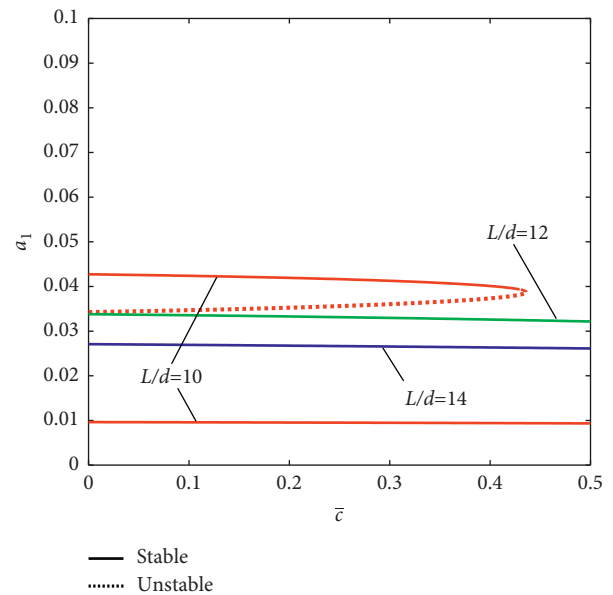
FIGURE 10: Amplitude versus damping coefficient with different ratios of length to diameter (σ = 2, $\bar{c}$ = 0.01, θ = 0°, case I).

one stable branch. For large values of $\bar{c}$ and large values of L/d, curves are always single-valued.

Figures 15–19 show the amplitude versus ply angle with different ratios of length to diameter, detuning parameter values, cutting force coefficients, damping coefficients, and rotating speeds, respectively ($\overline{\Omega} = \omega_1$). Similar to the cases in Figure 10 ~ 14, again, for some values of L/d, σ, K_f, or $\bar{c}$, multivalued curves can be observed.

Figures 20–24 show the amplitude versus cutting force coefficient with different ratios of length to diameter, detuning parameter values, ply angle, damping coefficients,

and rotating speeds, respectively. Again, when cutting force coefficient is less than the specified value, multivalued curves can be obtained for some values of L/d, σ, θ, $\bar{c}$, or $\overline{\Omega}$.

Figures 25–27 show the effects of ply sequences (see Table 3) on the frequency response curve, the amplitude versus dumping coefficient, and the amplitude versus cutting force coefficient, respectively. It can be seen from Figure 25 that the configuration A leads to the largest vibration amplitude, while the configuration C leads to the smallest vibration amplitude. This phenomenon can also be found in Figure 8 where the vibration amplitude increases with the
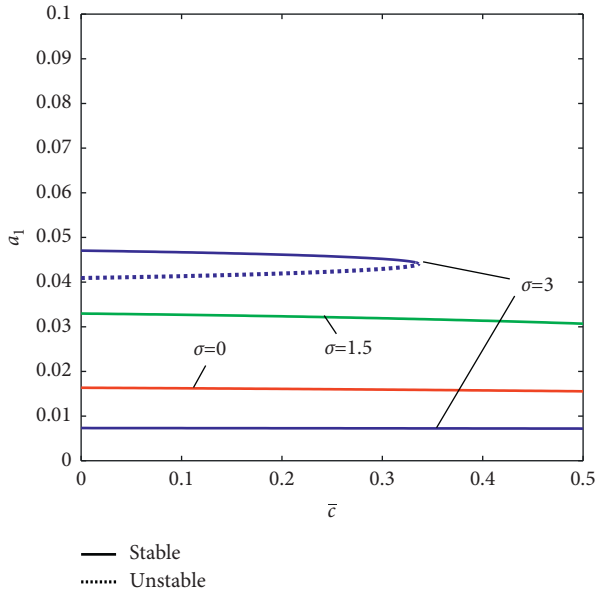
FIGURE 11: Amplitude versus damping coefficient with different detuning parameter values (L/d = 10, $\bar{c}$ = 0.01, θ = 0°, case I).
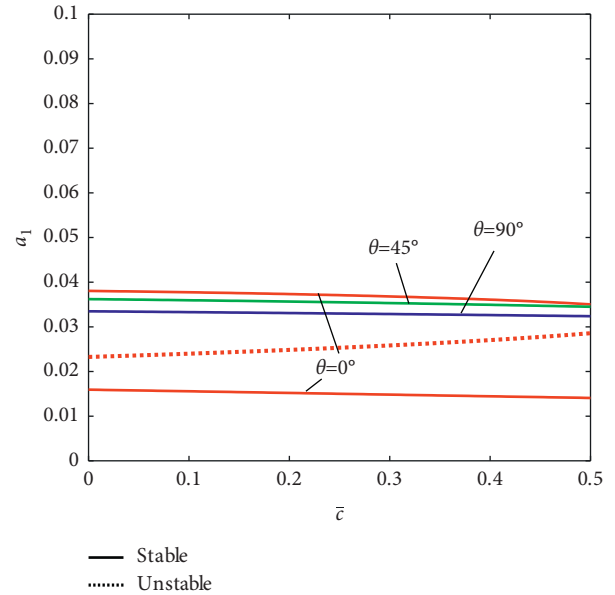
FIGURE 13: Amplitude versus damping coefficient with different ply angles (L/d = 10, σ = 2, case I).
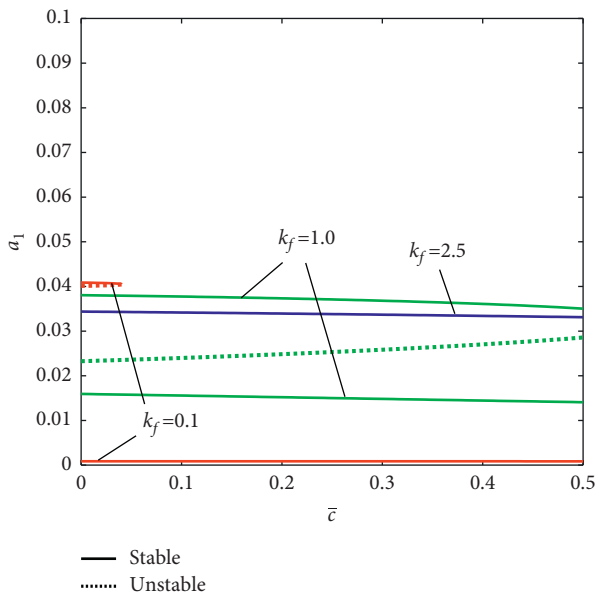
FIGURE 12: Amplitude versus damping coefficient with different cutting force coefficients (L/d = 10, σ = 2, θ = 0°, case I).
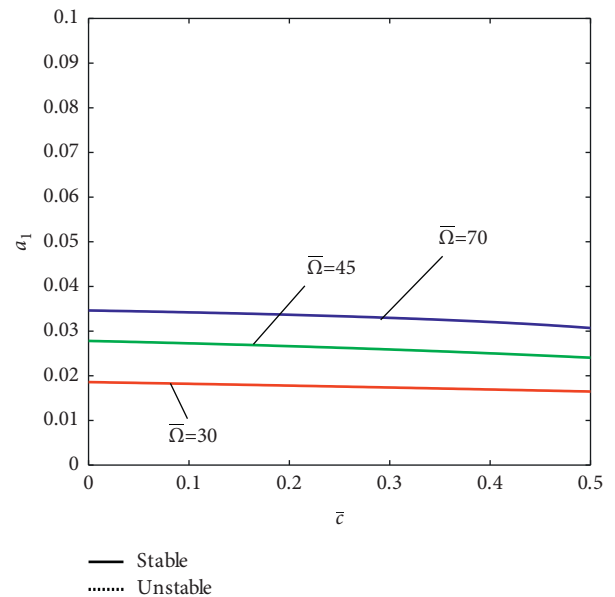
FIGURE 14: Amplitude versus damping coefficient with different rotating speed (L/d = 10, σ = 2, case I).

ply angle when using the same configuration. Again, it can be seen from Figures 26 and 27 that multivalued curves can be observed for some values of L/d, σ, K_f, or $\bar{c}$.

3.2.2. Case II. Figures 28–33 show the effects of ratio of length to diameter, structural damping, cutting force, ply angle, ply sequence, and rotating speed on frequency response curve, respectively, for the case $\bar{\Omega} = \omega_2$. As is observed, the frequency responses and effect of various parameters for the cutting system are similar to those in

case I; as ratio of length to diameter and structural damping increase, vibration amplitudes decrease. Furthermore, as cutting force coefficient, ply angle, and rotating speed increase, vibration amplitudes increase. However, for this case, vibration amplitudes are less than those of case I.

It should be noted that the equivalent damping of the cutting system is composed of the structural damping and the damping from regenerative chatter mechanism. The equivalent damping coefficient of case I can be expressed as
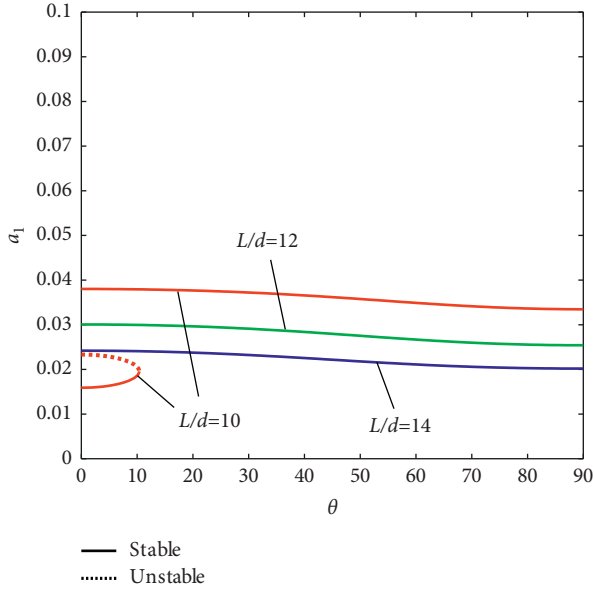
FIGURE 15: Amplitude versus ply angle with different ratios of length to diameter ($\bar{c} = 0.01$, $\sigma = -1.5$, case I).
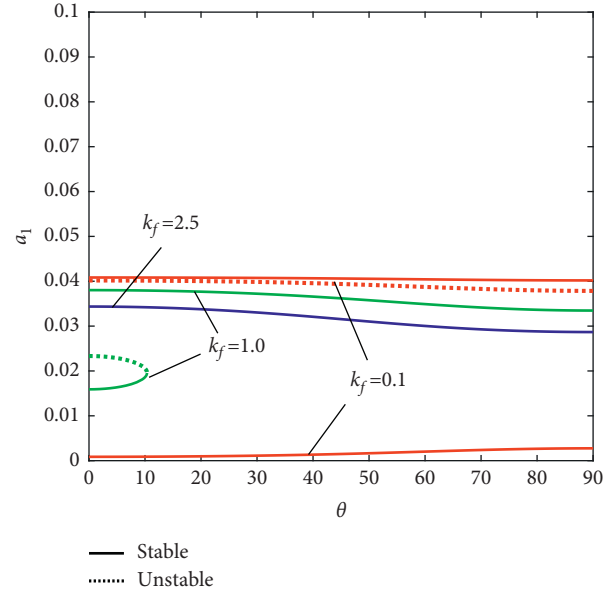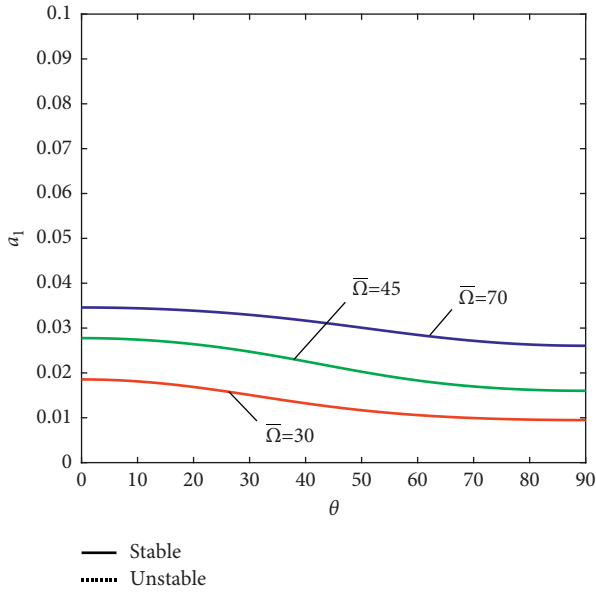

FIGURE 17: Amplitude versus ply angle with different cutting force coefficients (L/d = 10, $\bar{c} = 0.01$, $\sigma = 2$, case I).
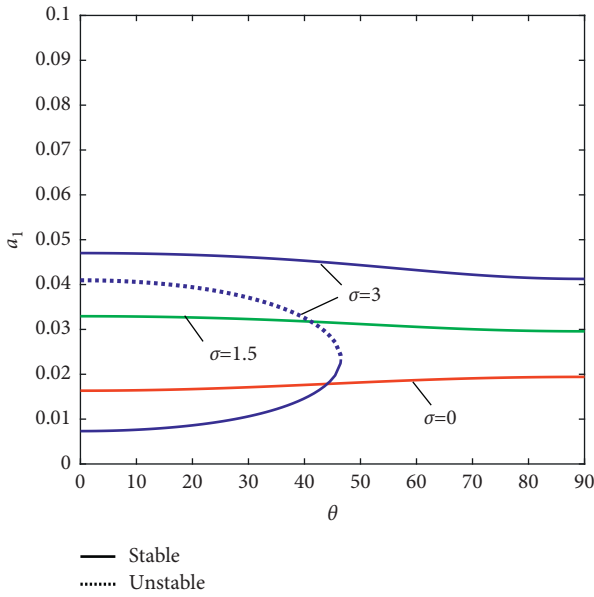
FIGURE 16: Amplitude versus ply angle with different detuning parameter values (L/d = 10, $\bar{c} = 0.01$, case I).
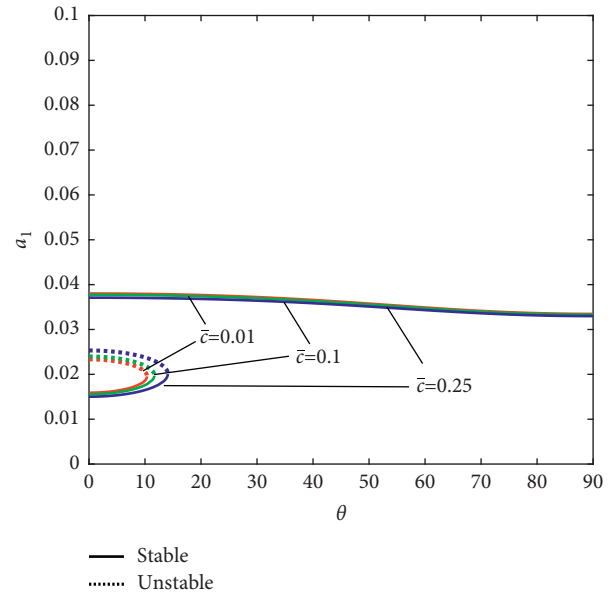
FIGURE 18: Amplitude versus ply angle with different damping coefficients (L/d = 10, $\sigma = 2$, case I).

$$c_{equiv1} = \bar{c} - \phi_1^2(1)\frac{N}{4\pi}\left[\left(\bar{\alpha}_0' + \bar{\beta}_0\right)\left(1 - \cos \omega_1 \bar{\tau}\right)\right.$$

$$\left. + \left(\bar{\beta}_0' - \bar{\alpha}_0\right)\sin \omega_1 \bar{\tau}\right]/\left[\omega_1 \int_0^1 \phi_1^2(x)dx\right]. \tag{45}$$

In addition, the equivalent damping coefficient of case II can be expressed as

$$c_{equiv2} = \bar{c} + \phi_1^2(1)\frac{N}{4\pi}\left[\left(\bar{\alpha}_0' + \bar{\beta}_0\right)\left(1 - \cos \omega_2 \bar{\tau}\right)\right.$$

$$\left. + \left(\bar{\alpha}_0 - \bar{\beta}_0'\right)\sin \omega_2 \bar{\tau}\right]/\left[\omega_2 \int_0^1 \phi_1^2(x)dx\right]. \tag{46}$$

Figures 34–38 show the effect of different parameters on the equivalent damping coefficients. As is observed, the

FIGURE 19: Amplitude versus ply angle with different rotating speeds (L/d = 10, $\bar{c} = 0.01$, $\sigma = 2$, case I).
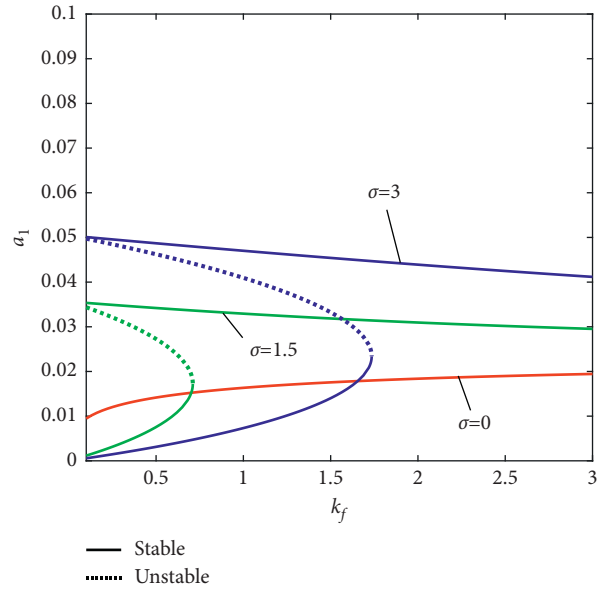
FIGURE 21: Amplitude versus cutting force coefficient with different detuning parameter values ($\theta = 0°$, $\bar{c} = 0.01$, L/d = 10, case I).
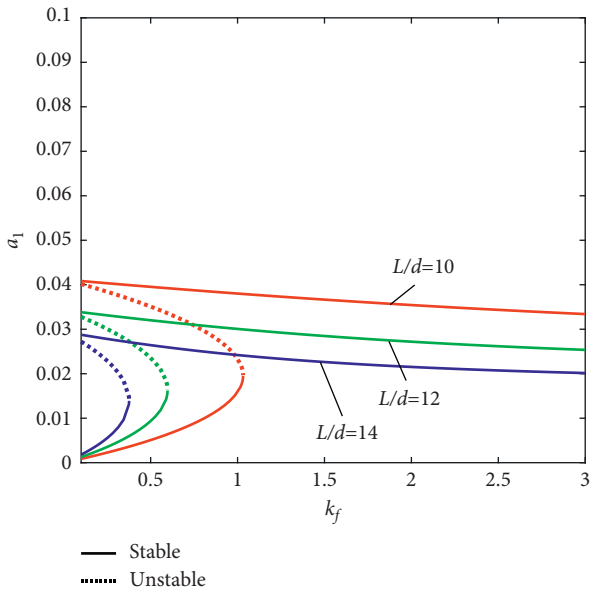
FIGURE 20: Amplitude versus cutting force coefficient with different ratios of length to diameter ($\theta = 0°$, $\bar{c} = 0.01$, $\sigma = 2$, case I).
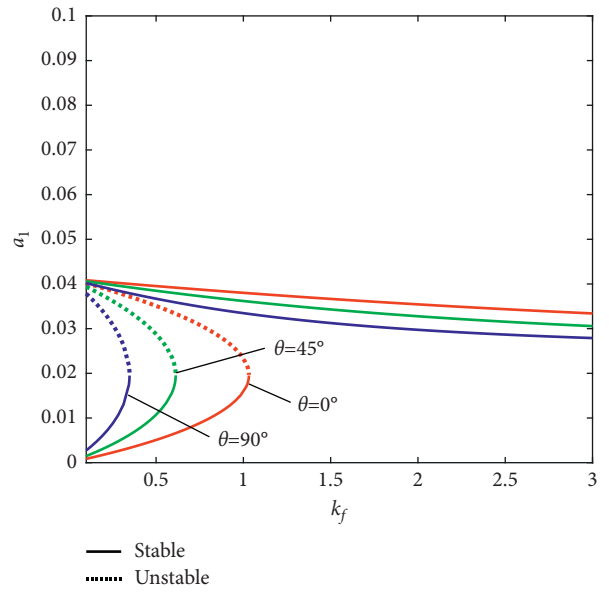
FIGURE 22: Amplitude versus cutting force coefficient with different ply angles ($\sigma = 2$, $\bar{c} = 0.01$, L/d = 10, case I).

equivalent damping coefficients of case I are always larger than those of case II. This explains the reason why vibration amplitudes of case I are larger than those of case II. It can be also seen that the equivalent damping coefficients increase with ratio of length to diameter, ply angle, cutting force, and

structural damping but decrease with rotating speed. Therefore, the increase of rotating speed leads to large vibration amplitudes, as shown in Figures 9 and 32. When rotating speed approaches infinity, the equivalent damping coefficient approaches the structural damping $\bar{c}$ (see Figure 38).
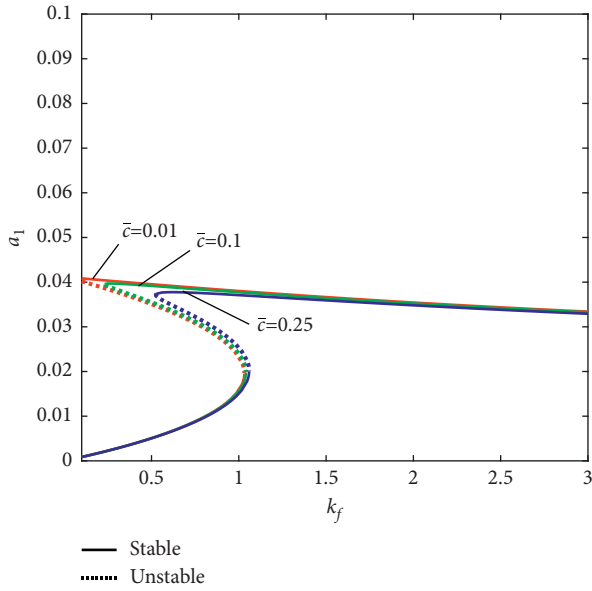
FIGURE 23: Amplitude versus cutting force coefficient with different damping coefficients ($\sigma = 2$, $\theta = 0°$, L/d = 10, case I).
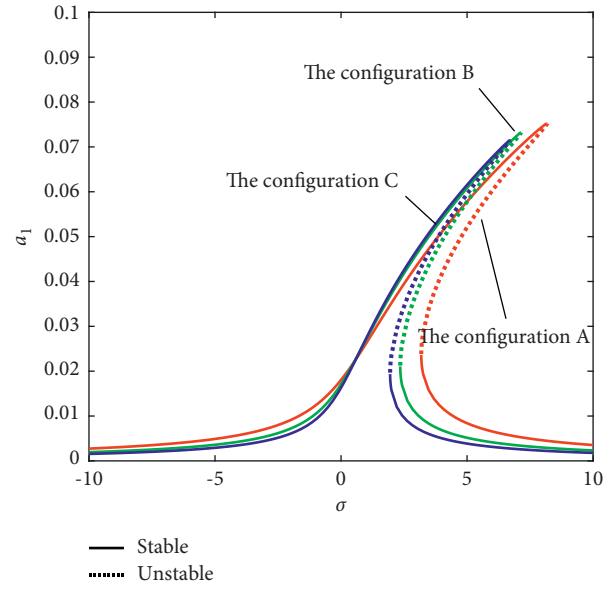
FIGURE 25: The frequency response curve with different ply sequences ($\bar{c} = 0.05$, L/d = 10, case I).
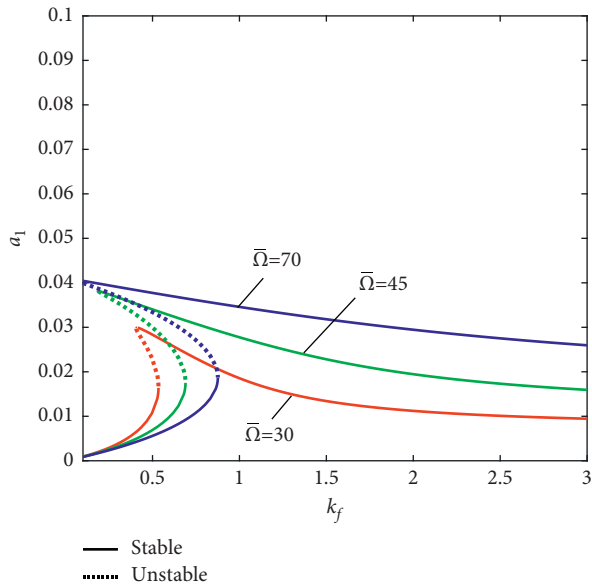
FIGURE 24: Amplitude versus cutting force coefficient with different rotating speeds ($\sigma = 2$, $\bar{c} = 0.01$, $\theta = 0°$, L/d = 10, case I).
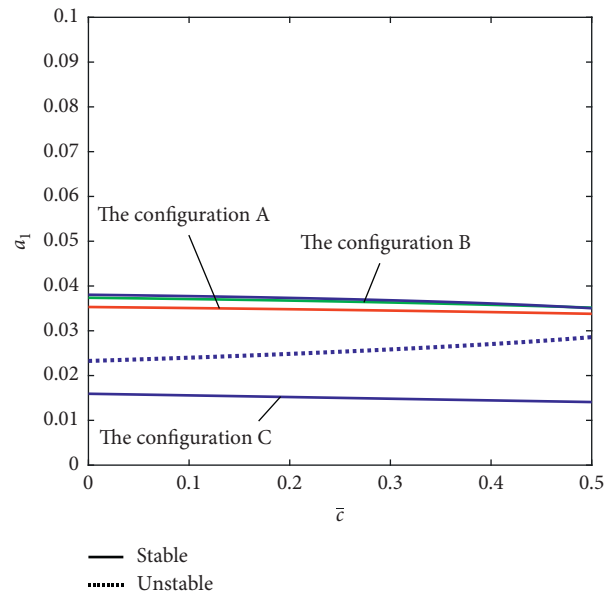
FIGURE 26: Amplitude versus dumping coefficient with different ply sequences ($\sigma = 2$, L/d = 10, case I).

Moreover, for some values of L/d, σ, K_f, $\bar{c}$, θ, or $\overline{\Omega}$, multivalued solutions can be found from the amplitude versus damping coefficient with different ratios of length to diameter, detuning parameter values, cutting force coefficients, ply angles, and rotating speeds, respectively (not shown).

TABLE 3: Configuration of composite.

Configuration	Sequence
A	$[90°/90°/0°]_s$
B	$[0°/90°/0°/0°/90°/0°]$
C	$[0°]_6$
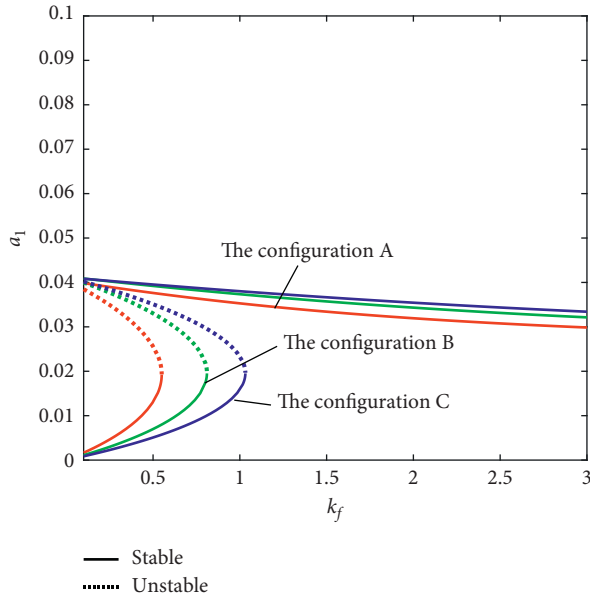
FIGURE 27: Amplitude versus cutting force coefficient with different ply sequences ($\bar{c} = 0.01$, $\sigma = 2$, L/d = 10, case I).
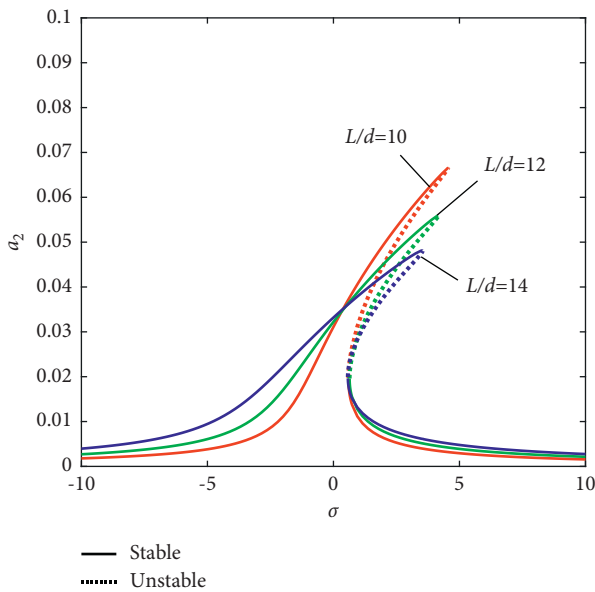

FIGURE 28: The effect of ratio of length to diameter on frequency response curve ($\theta = 0°$, $\bar{c} = 0.01$, case II).

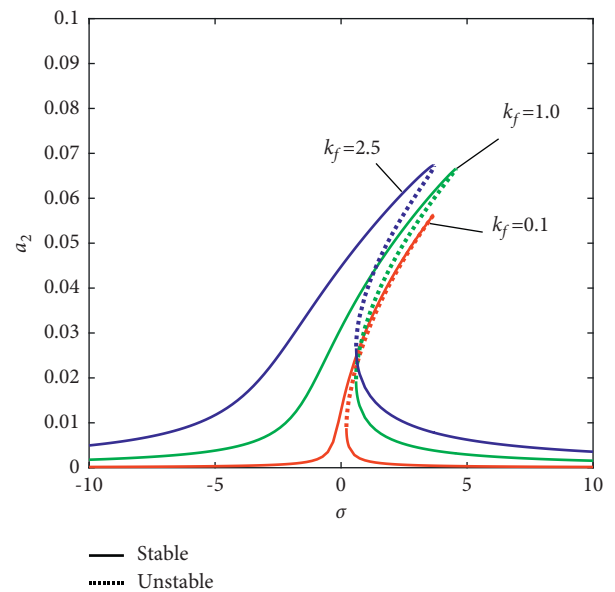FIGURE 29: The effect of structural damping on frequency response curve (L/d = 10, $\theta = 0°$, case II).

FIGURE 30: The effect of cutting force coefficient on frequency response curve (L/d = 10, $\theta = 0°$, $\bar{c} = 0.01$, case II).

Figure 39 shows the frequency response curve for the four cases. As is observed, the curves of cases I and III are very similar, except that the amplitude in case I is larger than that in case III. Likewise, the curves of cases II and IV are very similar, except that the amplitude in case II is larger than that in case IV.

3.2.3. Case III. For this case, the equivalent coefficient is identical with that in case I, but the amplitude of excitation force $(c_{f\varsigma_1}^2 + c_{f\eta_1}^2)/4$ in this case is lower than $(\bar{\varsigma}_2^2 + \bar{\eta}_2^2)$ in case I (e.g., using the same parameters L/d = 10, $\theta = 90°$, and $K_f = 3$, the amplitudes of excitation force are 0.2695 and 0.2532 for cases I and III, respectively). Therefore, generally,
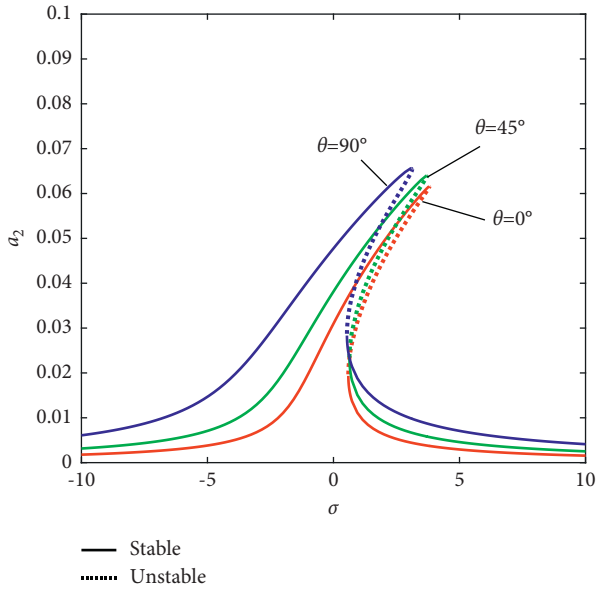
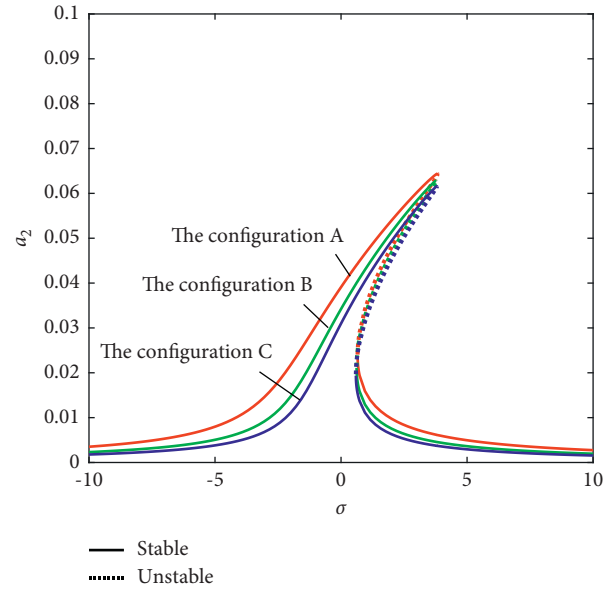FIGURE 31: The effect of ply angle on frequency response curve (L/d = 10, $\bar{c}$ = 0.01, case II).

FIGURE 33: Frequency response curve with different ply configurations ($\bar{c}$ = 0.05, L/d = 10, case II).
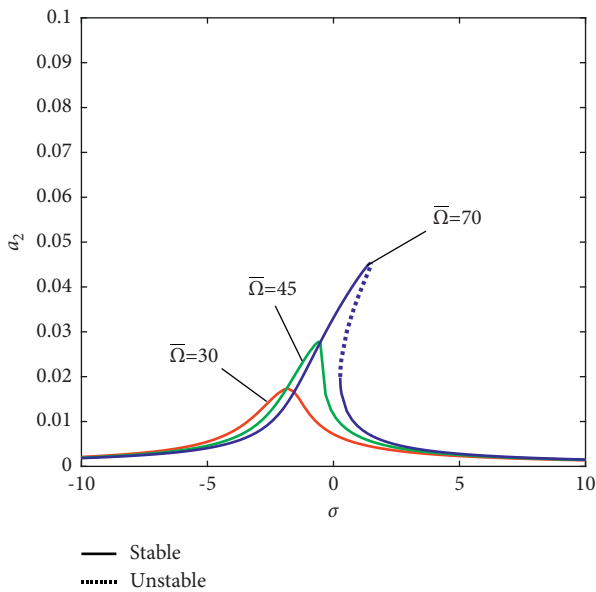

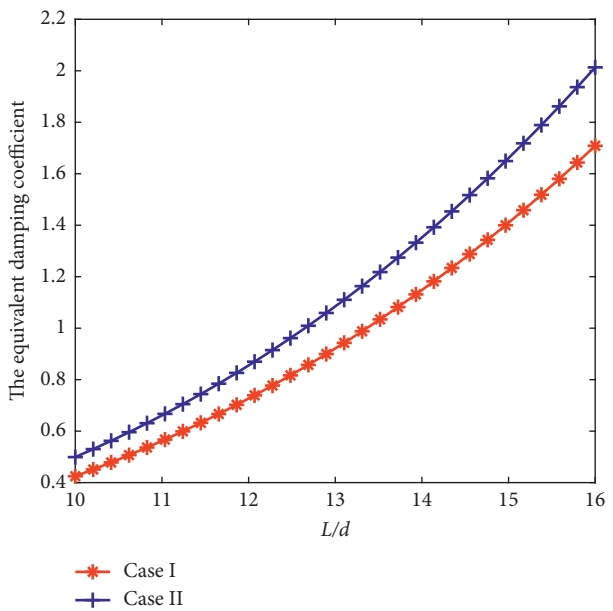FIGURE 32: The effect of rotating speed on frequency response curve (L/d = 10, $\bar{c}$ = 0.01, case II).

FIGURE 34: The equivalent damping coefficients versus ratio of length to diameter for cases I and II.

the behavior of nonlinear forced vibration in this case (see Figure 39) is similar to case I, despite having less vibration amplitudes compared with case I.

3.2.4. Case IV. For this case, the equivalent coefficient is identical with that in case II, and the amplitude of excitation force in this case is lower than that in in case II. Thus, under the same conditions, vibration amplitudes are generally

lower than those in case II. The results of case IV are not shown to save space.

In order to validate the calculated approximate solution using multiscale method, the numerical simulation results according to (17) are also displayed in Figures 40 and 41. These two calculated results using different methods are in good consistency.
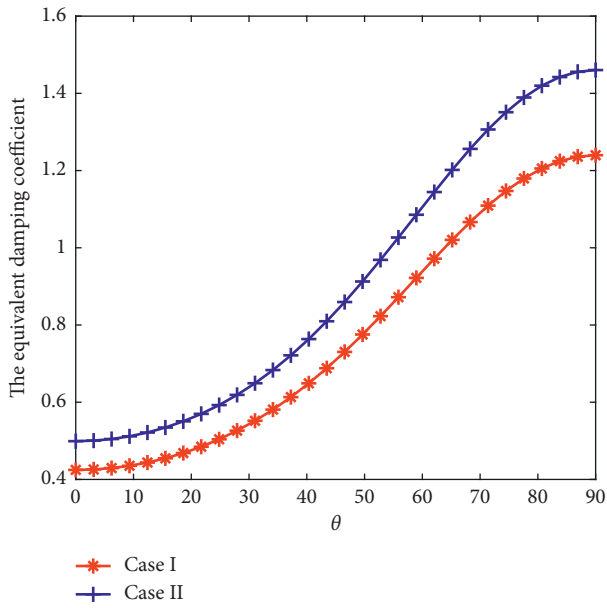
FIGURE 35: The equivalent damping coefficients versus ply angle for cases I and II.
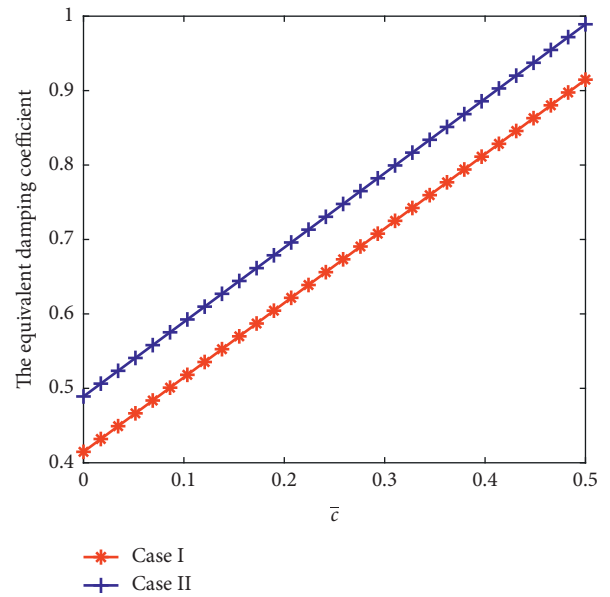

FIGURE 37: The equivalent damping coefficients versus structural damping for cases I and II.
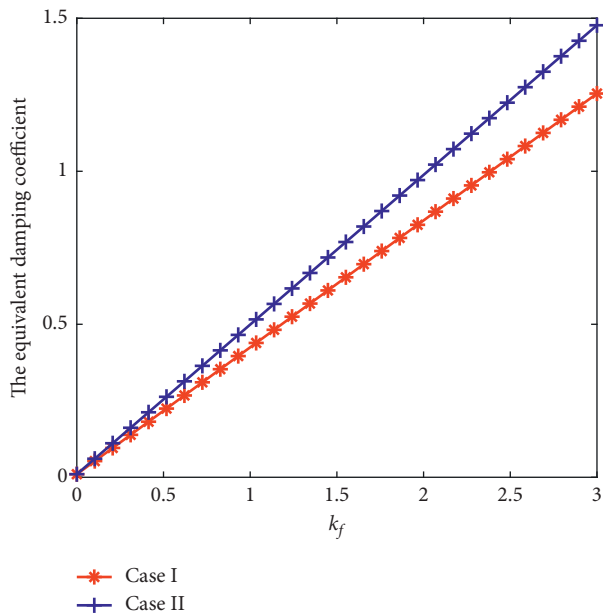

FIGURE 36: The equivalent damping coefficients versus cutting force for cases I and II.
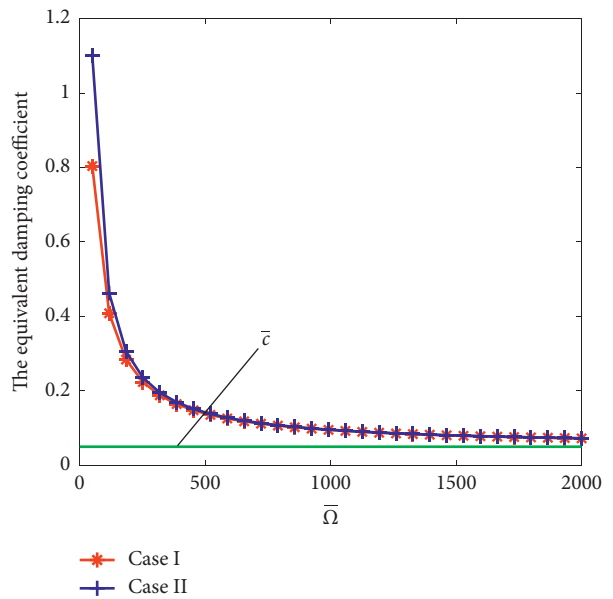

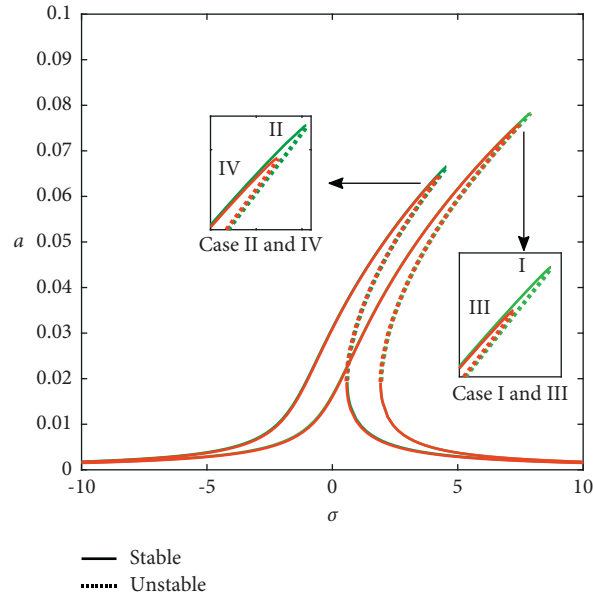FIGURE 38: The equivalent damping coefficients versus rotating speed for cases I and II.

FIGURE 39: The frequency response curve for the four cases (L/d = 10, $\bar{c}$ = 0.01, θ = 0°, $\overline{\Omega}$ = 100).
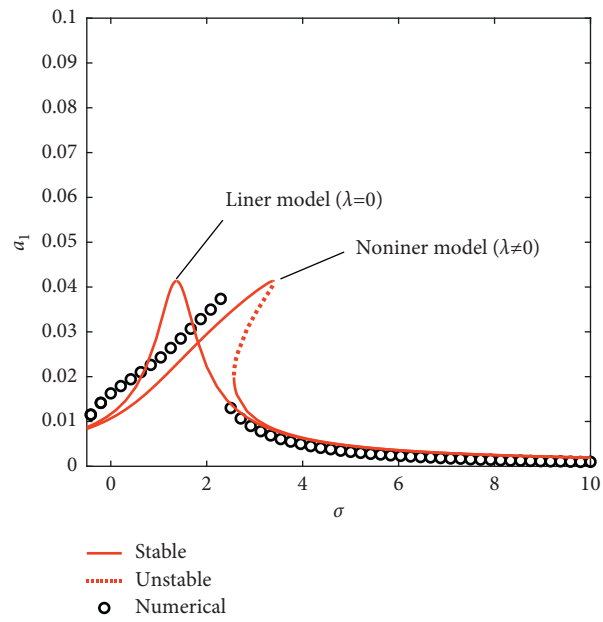

FIGURE 40: Comparison of results between the method of multiple scales and the numerical simulation (case I, L/d = 10, $\bar{c}$ = 0.03, θ = 0°, $\overline{\Omega}$ = 50, K_f = 1).
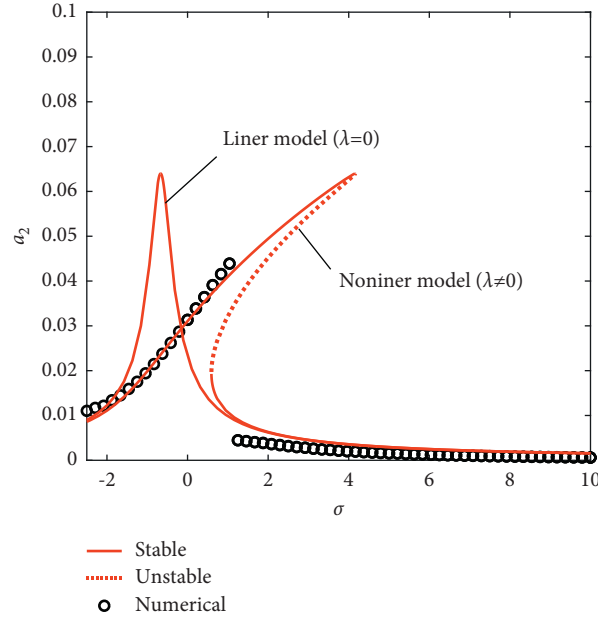
FIGURE 41: Comparison of results between the method of multiple scales and the numerical simulation (case II, L/d = 10, $\bar{c} = 0.03$, $\theta = 0°$, $\overline{\Omega}$ = 100, $K_f = 1$).

4. Conclusions

In this paper, a nonlinear dynamic model of the milling process with composite rotational cutting tool is presented. The cutting tool is simplified to a nonplanar bending Euler–Bernoulli beam, and the structural nonlinearity is attributed to the higher-order bending deformation of the cutting tool. A linear cutting force model considering regenerative mechanism, which includes time-delay terms and the first and second harmonic terms, is used. In addition, structural damping and gyroscopic effect are also considered. Nonlinear ordinary differential equations in the generalized coordinates are derived using the Hamilton principle and the Galerkin method. The lobe diagram of the cutting system is obtained. The multiscale method is used to construct the analytical approximate solutions of the forced vibration frequency response. It is found that, for all cases of primary resonance and superharmonic resonance, excitation of the forward (backward) mode does not produce the vibration responses in the backward (forward) mode because of not taking into account internal resonance in the proposed model. For primary and superharmonic resonance conditions, the effective nonlinearity of the cutting system with higher-order bending deformation rotating composite cutting tool is of a hard type. Jump phenomenon and multivalued solutions can be observed.

The influence of higher-order bending deformation causes the frequency response curve to bend more strongly toward right when ratio of length to diameter increases. The study also finds that the vibration amplitudes of the cutting tool increase with cutting force or ply angle. It can be seen that the damping of the cutting system has a significant influence on the vibration amplitude of the composite cutting tool. The damping capacities of the cutting system can be measured by the two different equivalent damping coefficients c_{equiv1} and c_{equiv2} which include the structural damping and the damping from regenerative chatter mechanism. Cases I and III have the same equivalent damping coefficient c_{equiv1}, and cases II and IV have the same equivalent damping coefficient c_{equiv2}. It has been found that c_{equiv2} is larger than c_{equiv1}, so the vibration amplitudes of case I are larger than those of case II. In addition, for all resonant cases, as rotating speed decreases or structural damping increases, the equivalent damping coefficient is strengthened, and consequently less vibration amplitudes are observed. Therefore, from this point of view, low rotating speeds are preferable to keep vibration amplitudes small. [38].

Abbreviations

T:	Kinetic energy
L:	Length of the cutting tool
t:	Time
ρ:	Density
A:	Cross-sectional area
I:	Second moment of area of the beam cross section
v, w:	Transverse deflections of the shaft element
x, y, z:	Variable coordinates
ψ_y, ψ_z:	Rotation angles of the cross section around the y and z axes
Ω:	Rotating speed of the shaft
$\overline{Q}_{11}$:	Off-axis stiffness coefficient of the kth layer for the composite cutting tool
U:	Potential energy
W_c:	Rayleigh dissipative energy function of the cutting tool
c:	Structural damping coefficient
δ:	Variational operator

δW: Virtual work of the cutting force
F_y, F_z: Linear regenerative cutting forces
τ: Delay time of milling process
N: The number of teeth
K_{tc}: Cutting force coefficients in the tangential directions
K_{te}: Edge force coefficients in the tangential directions
K_{rc}: Cutting force coefficients in the radial directions
K_{re}: Edge force coefficients in the radial directions
a: Axial cutting depth
c_f: Feed per tooth per revolution
$(EI)_{\text{equiv}}$, $(EA)_{\text{equiv}}$: Equivalent bending and tensile stiffness of the cutting tool
$(\rho I)_{\text{equiv}}$, $(m)_{\text{equiv}}$: Equivalent diametrical mass moment of inertia and equivalent mass per unit length
ρ_k: Density of the kth layer
r_k, r_{k+1}: Inner diameter and outer diameter of the kth layer
$\phi_1(\overline{x})$: Mode function
ω_1, ω_2: Forward and backward whirling frequencies
ε: Small parameter
i: $\sqrt{-1}$.

Appendix

A. The Stain Energy of the Composite Cutting Tool

If the torsional deformation is negligible, the bending displacements of the composite cutting tool in x, y, and z directions are as follows:

$$u_x = -z\psi_y + y\psi_z, u_y = v, u_z = w. \tag{A.1}$$

The strain in the x direction is

$$\varepsilon_{xx} = \varepsilon_l + \varepsilon_{nl}, \tag{A.2}$$

where

$$\varepsilon_l = -z\frac{\partial \psi_y}{\partial x} + y\frac{\partial \psi_z}{\partial x}, \varepsilon_{nl} = \frac{1}{2}\psi_y^2 + \frac{1}{2}\psi_z^2, \tag{A.3}$$

where ε_l and ε_{nl} are the linear strain and the nonlinear strain generated in high-order bending deformation, respectively.

Bending energy for the composite cutting tool can be expressed as

$$U = \frac{1}{2}\int_0^L \iint_A (\sigma_{xx}\varepsilon_{xx})dAdx. \tag{A.4}$$

The elastic stress-strain relations of the laminate cutting tool can be expressed as

$$\sigma_{xx} = \overline{Q}_{11}\varepsilon_{xx}. \tag{A.5}$$

Employing (A.2), (A.3), and (A.5), (A.4) can be rewritten as

$$U = \frac{1}{2}\int_0^L \iint_A \overline{Q}_{11}\left(z^2\left(\frac{\partial \psi_y}{\partial x}\right)^2 + y^2\left(\frac{\partial \psi_z}{\partial x}\right)^2 - 2yz\frac{\partial \psi_y}{\partial x}\frac{\partial \psi_z}{\partial x} + \frac{1}{4}\psi_y^4 + \frac{1}{4}\psi_z^4 + \frac{1}{2}\psi_y^2\psi_z^2 - 2\left(z\frac{\partial \psi_y}{\partial x} + y\frac{\partial \psi_z}{\partial x}\right)\left(\frac{1}{2}\psi_y^2 + \frac{1}{2}\psi_z^2\right)\right)^2 dAdx. \tag{A.6}$$

Due to the symmetry of the cross section, the third and seventh terms in the above equation are equal to zero.

Therefore, the strain energy of the composite cutting tool can be reduced as follows:

$$U = \frac{(EI)_{\text{equiv}}}{2}\int_0^L \left(\left(\frac{\partial \psi_y}{\partial x}\right)^2 + \left(\frac{\partial \psi_z}{\partial x}\right)^2\right)dx + \frac{(EA)_{\text{equiv}}}{2}\int_0^L \left(\frac{1}{4}\psi_y^4 + \frac{1}{4}\psi_z^4 + \frac{1}{2}\psi_y^2\psi_z^2\right)dx. \tag{A.7}$$

B. The Expression of the Off-Axis Stiffness Coefficient

The off-axis stiffness coefficient of the kth layer for the composite cutting tool is defined as

$$\overline{Q}_{11} = C_{11}\cos^4\theta^{(k)} + C_{22}\sin^4\theta^{(k)} + 2(C_{12} + 2C_{66})\sin^2\theta^{(k)}\cos^2\theta^{(k)}, \tag{B.1}$$

where $\theta^{(k)}$ is the layer angle of each layer of the material. The expressions of C_{11}, C_{12}, C_{22}, and C_{66} are as follows:

$$C_{11} = \frac{E_{11}}{1 - \nu_{12}\nu_{21}}, C_{12} = \frac{\nu_{12}E_{11}}{1 - \nu_{12}\nu_{21}} = \frac{\nu_{21}E_{22}}{1 - \nu_{12}\nu_{21}}, C_{22} = \frac{E_{22}}{1 - \nu_{12}\nu_{21}}, C_{66} = C_{12}, \tag{B.2}$$

where

$$v_{21} = \frac{v_{12}E_{11}}{E_{22}}. \tag{B.3}$$

Data Availability

The data used to support the findings of this study are included within the article.

Conflicts of Interest

The authors declare that they have no conflicts of interest.

Acknowledgments

References

[1] K. Seto and N. Tominari, "Effect of a variable stiffness-type dynamic damper on machine tools with long overhung ram," *Bulletin of JSME*, vol. 19, no. 137, pp. 1270–1277, 1976.

[2] D. J. P. Hartog, *Mechanical Vibrations*, McGraw-Hill, New York, 1956.

[3] S. Ema and E. Marui, "Suppression of chatter vibration of boring tools using impact dampers.International," *Journal of Machine Tools and Manufacture*, vol. 40, no. 8, pp. 1141–1156, 2008.

[4] S. Nagano, T. Koizumi, T. Fujii, N. Tsujiuchi, H. Ueda, and S. Kobe, "Development of a composite boring bar. Compos Structures," *Composite Structures*, vol. 38, pp. 531–539, 1997.

[5] D. G. Lee, H. Y. Hwang, and J. K. Kim, "Design and manufacture of a carbon fiber epoxy rotating boring bar," *Composite Structures*, vol. 60, pp. 115–124, 2003.

[6] S. Ghorbani, V. A. Rogov, A. Carluccio, and P. S. Belov, "The effect of composite boring bars on vibration in machining process," *International Journal of Advanced Manufacturing Technology*, vol. 105, no. 1-4, pp. 1157–1174, 2019.

[7] F. Taylor, "On the art of cutting metals," *Trans. ASME*, vol. 28, pp. 31–350, 1907.

[8] S. A. Tobias and W. Fishnick, "The chatter of lathe tools under orthogonal cutting conditions," *Transactions of the American Society of Mechanical Engineers*, vol. 80, pp. 1079–1086, 1958.

[9] H. E. Merritt, "Theory of self-excited machine tool chatter, condition to machine tool chatter research-1," *Transactions of the American Society of Mechanical Engineers, Journal of Engineering for Industry*, vol. 87, pp. 447–454, 1965.

[10] S. Kato and E. Marui, "On the cause of regenerative chatter due to workpiece deflection," *Transactions of the American Society of Mechanical Engineers, Journal of Engineering for Industry*, vol. 96, pp. 179–186, 1974.

[11] D. W. Wu and C. R. Li, "An analytical model of cutting dynamics," *Transactions of the American Society of Mechanical Engineers, Journal of Engineering for Industry*, vol. 107, pp. 107–188, 1985.

[12] Y. Altintas, *Manufacturing Automation, Metal Cutting Mechanics, Machine Tool Vibrations, and CNC Design*, Cambridge University Press, New York, 2000.

[13] E. Budak and Y. Altintas, "Analytical prediction of chatter stability in milling. Part I: general formulation," *Trans. ASME, Journal of Dynamic Systems, Measurement, and Control*, vol. 120, pp. 22–30, 1998.

[14] E. Budak and Y. Altintas, "Analytical prediction of chatter stability in milling. Part II: application of the general formulation to common milling systems," *Trans. ASME, Journal of Dynamic Systems, Measurement, and Control*, vol. 120, pp. 31–36, 1998.

[15] N. H. Hanna and S. A. Tobias, "A theory of nonlinear regenerative chatter," *Transactions of American Society of Mechanical Engineers, Journal of Engineering for Industry*, vol. 96, pp. 247–255, 1974.

[16] L. Vela-Martinez, J. C. Jáuregui-Correa, O. M. González-Brambila, and H. R. Gilberto, "Instability conditions due to structural nonlinearities in regenerative chatter," *Nonlinear Dynamics*, vol. 56, pp. 415–427, 2009.

[17] N. Deshpande and M. S. Fofana, "Nonlinear regenerative chatter in turning," *International Journal of Computer Integrated Manufacturing*, vol. 17, pp. 107–112, 2001.

[18] G. Stepan, T. Insperger, and R. Szalai, "Delay, parametric excitation, and the nonlinear dynamics of cutting process," *International Journal of Bifurcation and Chaos*, vol. 15, no. 9, pp. 2783–2798, 2005.

[19] J. R. Pratt, *Vibration Control for Chatter Suppression*, Ph.D. Thesis, Virginia Polytechnic Institute and State University, Blacksburg, VA, 1997.

[20] H. Moradi, M. R. Movahhedy, and G. Vossoughi, "Bifurcation analysis of milling process with tool wear and process damping: regenerative chatter with primary resonance," *Nonlinear Dynamics*, vol. 70, no. 1, pp. 481–509, 2012.

[21] H. Moradi, G. Vossoughi, M. R. Movahhedy, and T. A. Mohammad, "Forced vibration analysis of the milling process with structural nonlinearity, internal resonance, tool wear and process damping effects," *International Journal of Non-linear Mechanics*, vol. 54, pp. 22–34, 2013.

[22] H. Moradi, M. R. Movahhedy, and G. Vossoughi, "Dynamics of regenerative chatter and internal resonance in milling process with structural and cutting force nonlinearities," *Journal of Sound and Vibration*, vol. 331, pp. 3844–3865, 2012.

[23] P. N. Rao, U. R. K. Rao, and J. S. Rao, "Towards improved design of boring bars part 1: dynamic cutting force model with continuous system analysis for the boring bar," *Journal of Machine Tools Manufacture*, vol. 28, no. 1, pp. 33–44, 1988.

[24] L. Andren, L. Hakansson, A. Brandt, and I. Claesson, "Identification of dynamic properties of boring bar vibrations in a continuous boring operation," *Journal of Mechanical Systems and Signal Processing*, vol. 18, no. 4, pp. 869–901, 2004.

[25] L. Andren, L. Hakansson, A. Brandt, and I. Claesson, "Identification of motion of cutting tool vibration in a continuous boring operation-correlation to structural properties," *Journal of Mechanical Systems and Signal Processing*, vol. 18, pp. 903–927, 2004.

[26] B. Moetakef-Imani and N. Z. Yussefian, "Dynamic simulation of boring process," *International Journal of Machine Tools and Manufacture*, vol. 49, pp. 1096–1103, 2009.

[27] M. Sortino, G. N. Totis, and F. Prosperi, "Modeling the dynamic properties of conventional and high-damping boring bars," *Mechanical Systems and Signal Processing*, vol. 34, pp. 340–352, 2013.

[28] B. Huang, "The drilling vibration behavior of a twisted microdrill," *ASME, Journal of Manufacturing Science and Engineering*, vol. 126, pp. 719–726, 2004.

[29] S. Filiz and O. B. Ozdoganlar, "Micro-end mill dynamics including the actual fluted geometry and setup errors-part I:

model development and numerical solution," *ASME, Journal of Manufacturing Science and Engineering*, vol. 130, no. 03, pp. 11–19, 2008.

[30] M. R. Movahhedy and P. Mosaddegh, "Prediction of chatter in high speed milling including gyroscopic effects," *International Journal of Machine Tools and Manufacture*, vol. 46, no. 9, pp. 996–1001, 2005.

[31] S. A. Tajalli, M. R. Movahhedy, and J. Akbari, "Chatter instability analysis of spinning micro-end mill with process damping effect via semi-discretization approach," *Acta Mechanics*, vol. 225, pp. 715–734, 2014.

[32] C. J. Li, A. G. Ulsoy, and W. J. Endres, "The effect of flexible-tool rotation on regenerative instability in machining," *Journal of Manufacturing Science and Engineering*, vol. 125, no. 1, pp. 39–47, 2003.

[33] W. Kim, A. Argento, and R. A. Scott, "Forced vibration and dynamic stability of a rotating tapered composite Timoshenko shaft: bending motions in end-milling operations," *Journal of Sound and Vibration*, vol. 246, no. 4, pp. 583–600, 2001.

[34] M. R. Shad, G. Michon, and A. Berlioz, "Modeling and analysis of nonlinear rotordynamics due to higher order deformation in bending," *Applied Mathematical Modelling*, vol. 35, pp. 2145–2159, 2011.

[35] A. H. Nayfeh and P. F. Pai, *Linear and Nonlinear Structural Mechanics*, John Wiley & Sons, New York, 2004.

[36] A. H. Nayfeh, *Introduction to Perturbation Techniques*, Wiley-Interscience, New York, 1981.

[37] D. A. Saravanos, D. Varelis, T. S. Plagianakos, and N. Chrysochoidis, "A shear beam finite element for the damping analysis of tubular laminated composite beams," *Journal of Sound and Vibration*, vol. 291, pp. 802–823, 2006.

[38] G. Tlusty, *Manufacturing Process and Equipment*, Prentice-Hall, Englewood, 2000.